Aus dem
Department für Augenheilkunde
Forschungsinstitut für Augenheilkunde

Investigating the use of mycophenolic acid for the treatment of Retinitis Pigmentosa

**Inaugural-Dissertation
zur Erlangung des Doktorgrades
der Medizin**

**der Medizinischen Fakultät
der Eberhard Karls Universität
zu Tübingen**

vorgelegt von

Jenisch, Peter Klaus

2025

Dekan:	Professor Dr. Bernd Pichler
1. Berichterstatter:	Professor Dr. François Paquet-Durand
2. Berichterstatter:	Professorin Dr. E. Reisinger
Tag der Disputation	28.02.2025

Table of contents

List of Figures

List of Tables

Abbreviations

Abbreviation	Explanation
µg	Microgram
µl	Microliter
µM	Micromolar
AB	Antibody
Arr3	Cone arrestin
BM	Basal R16 Medium
BSA	Bovine serum albumin
Ca^{2+}	Calcium
cGMP	Cyclic guanosine monophosphate
CM	Complete Medium
CNGC	Cyclic nucleatide-gated channel
DAPI	4’,6-diamidino-2-phenylindole
DMSO	Dimethyl sulfoxide
DNA	Deoxyribose nucleic acid
ERG	Electroretinography
FBS	Fetal bovine serum
Fig.	Figure
GCL	Ganglion cell layer
GDP	Guanosine diphosphate
GMP	Guanosine monophosphate
GTP	Guanosine triphosphate
h	Hour
HDAC	Histone deacetylase
IMPDH1	Inosine monophosphate dehydrogen-ase 1
INL	Inner nuclear layer
IPL	Inner plexiform layer
IRD	Inherited retinal dystrophy
IS	Inner segment
K+	Potassium
KO	Knockout
LAF	Laminar Air Flow
LCA	Leber congenital amaurosis
Min	Minute
MPA	Mycophenolic acid
MMF	Mycophenolate mofetil
mRNA	Messenger RNA
Na^{+}	Sodium
NAD^{+}	Nicotinamide adenine dinucleotide
NADH	NAD + hydrogen (H)
NDS	Normal donkey serum
ng	nanogram
NGS	Normal goat serum

ONL	Outer nuclear layer
OPL	Outer plexiform layer
OS	Outer segment
P	Post-natal day
PAR	Poly-ADP ribose
PARP	Poly-ADP ribose polymerase
PGCE	Particulate Guanylate Cyclase E
PB	Phosphate buffer
PBS	Phosphate buffered saline
PBST	Phosphate buffered saline with chemical detergent
PCR	Polymerase chain reaction
PDE6	Phosphodiesterase 6
PDE6α	Phosphodiesterase 6 α-subunit
PDE6β	Phosphodiesterase 6 β-subunit
PKG	Protein kinase G
rd1	Retinal degeneration 1
rd2	Retinal degeneration 2
rd10	Retinal degeneration 10
RetGC	Retinal guanylate cyclase
RP	Retinitis Pigmentosa
RPE	Retinal pigment epithelium
RT	Room temperature
SNARE	Soluble N-ethylmaleimide-sensitive-factor attachment receptor
T3	Triiodothyronine
TBS	Tris buffered saline
TUNEL	Terminal deoxynucleotidyl transferase dUTP nick end labelling
Vit.	Vitamin
V	Volt
VEGF	Vascular endothelial growth factor
VZV	Vitreous chamber volume
WT	Wild-type

1 Introduction

1.1 The eye and retina

The mammalian eye is an exceptionally important sensory organ for humans. It provides us with the ability to process visible light and enables a connection to our surroundings via perception of objects and organisms, sense of depth and balance. Furthermore, it allows the use and interpretation of gesticulation and facial expressions in interpersonal communication.

As seen on the left side of Figure 1 the eye has a spherical shape and is made up of different layers each contributing to a reliable function of the eye. The muscles for movement, sclera for stability and protection, choroid for vascularization. Along the optical axis (yellow dashed line), the refractive cornea and lens focus images onto the light sensitive retina. The iris modifies the amount of light entering the eye by expanding and reducing the pupil area. The transparent vitreous body transmits light and fills the inside of the eye to maintain its shape.

The right side of Figure 1 illustrates the 10 retinal layers and their respective cell types, as well as the direction of light going through the retina before reaching the photoreceptor cells. The Photoreceptors reside in the outer retina and convert light via the phototransduction cascade into an electrochemical message that is passed on towards 2nd order neurons in the inner retina. About 130 million photoreceptor cells are present in the human outer retina, which is made up of mainly rods and harbors only about 3% of cone photoreceptors. The latter are concentrated in the fovea, thinning out into the macula and further periphery (Szel et al., 1992). Rods and cones fulfill different tasks when light interacts with them. Three types of cone photoreceptors react to different wavelengths of light and provide high resolution photopic images in good lighting conditions. Rod photoreceptors have a higher sensitivity to light stimuli, enable scotopic vision for dim light vision and recognition of silhouettes in such a low light environment.

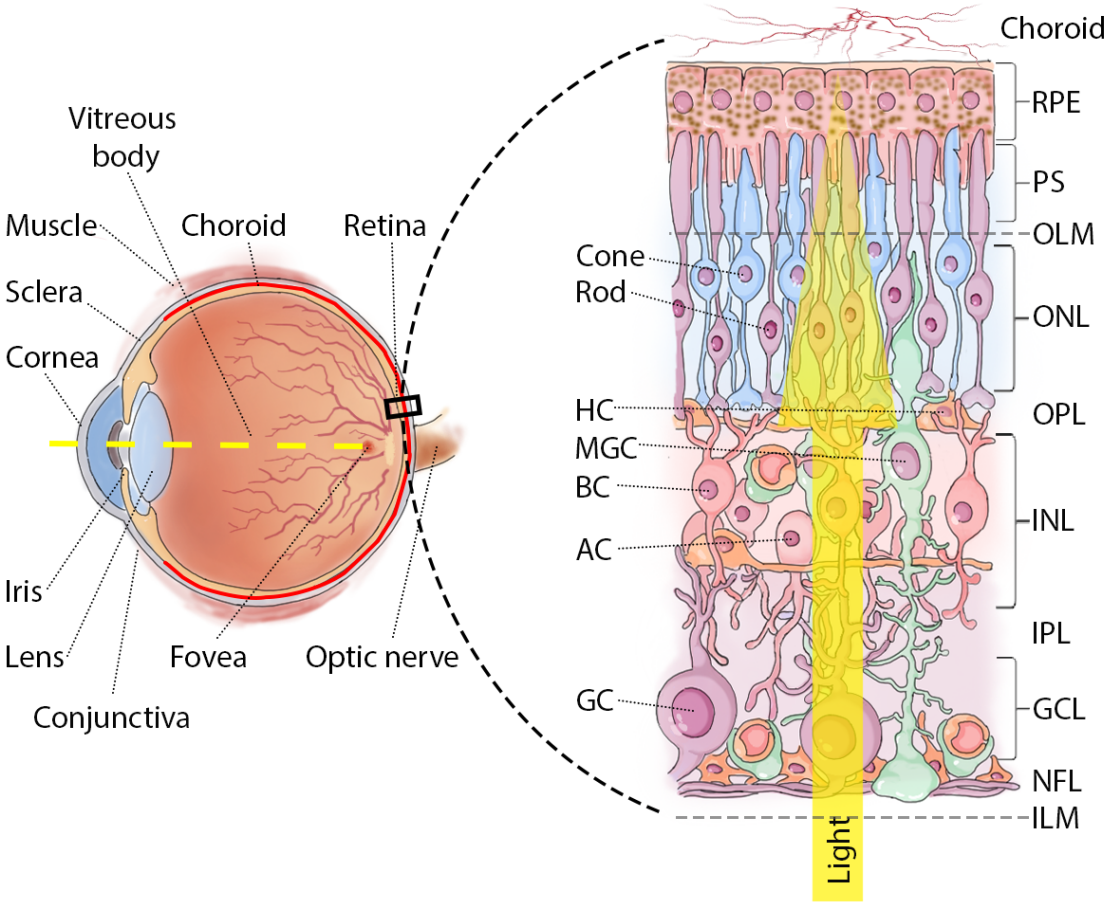

Figure 1: Schematic drawing of the eye and retinal cellular structure

Anatomic representation of the mammalian eyeball on the left. The right side illustrates the pathway that incoming light takes through the retinal layers until reaching the photoreceptors and starting the visual transduction. Retinal pigment epithelium (RPE), photoreceptor segments (PS), outer limiting membrane (OLM), outer plexiform layer (OPL), inner nuclear layer (INL), inner plexiform layer (IPL), ganglion cell layer (GCL), nerve fiber layer (NFL), inner limiting membrane (ILM), horizontal cell (HC), Müller glial cell (MGC), bipolar cell (BC), amacrine cell (AC), ganglion cell (GC). Drawing of the eye and retina modified after an original drawing by Yu Zhu.

1.1.1 Visual signal transduction

In rod photoreceptors, phototransduction includes a number of key steps (Figure 2) Light reaches through the eye and the layers of retina to the opsin complex, isomerizing 11-*cis*-retinal to all-*trans*-retinal in photoreceptor outer segments. This triggers a biochemical cascade that dramatically amplifies the light signal. Photoreceptors are depolarized while unstimulated with a membrane potential of approximately - 40 mV. A conformation change from rhodopsin to metarhodopsin II then activates the G protein transducin, enabling it to bind guanosine triphosphate (GTP) instead of guanosine diphosphate (GDP). The binding part, *i.e.* the alpha subunit of transducin, disconnects from transducin to bind to a subunit of phosphodiesterase 6 (PDE6) and triggers its activity. PDE6 hydrolyzes the second messenger cyclic guanosine monophosphate (cGMP) to guanosine monophosphate (GMP), lowering the intracellular cGMP level, which in turn closes cyclic nucleotide gated channels (CNGC) responsible for sodium influx (Arshavsky et al., 2002). This causes a hyperpolarization down to about -75 mV, as potassium still leaves the cell, and closes voltage-gated calcium channels. In the photoreceptor synapse, decreasing intracellular calcium levels lead to less glutamate containing soluble N-ethylmaleimide-sensitive-factor attachment receptor (SNARE) vesicles fusing with the cell membrane, decreasing the release of the neurotransmitter glutamate. This leads to a de- or hyperpolarization of the following bipolar cells depending on their glutamate receiving receptors (Schmitz and Witkovsky, 1997, Grossman et al., 1994).

Part of the visual cycle is the recovery of the initial membrane potential, cascade proteins and 11-*cis*-retinal in the opsin complex. All-*trans*-retinol is transported into the RPE where retinyl esters are restored to 11-*cis*-retinol. After being restored to 11-*cis*-retinal, it is then transported back into the photoreceptors to be reincorporated into the opsin complex (Moiseyev et al., 2005).

The chromophores of cones are similar to those of the rods. We label three different cone types with “blue”, “red” and “green”, according to their absorption peaks. Furthermore, all cones are stimulated by adjacent light wavelengths, enabling the perception of light of different colors, including yellow and purple.

During phototransduction a chemical stimulus is converted into an electrical one, which is then modulated and forwarded by bipolar, horizontal, and amacrine cells. Reaching the retinal ganglion cells, the signal is transformed into an action potential and transmitted to the brain via the optic nerve. Since there are more photoreceptors than ganglion cells, the modulation by the interneurons leads to a convergence of input in order to bring the signals together. This process does not take place in the cone dominated fovea, where each cone is connected to a bipolar and via this to a ganglion cell (1:1:1 connectivity).

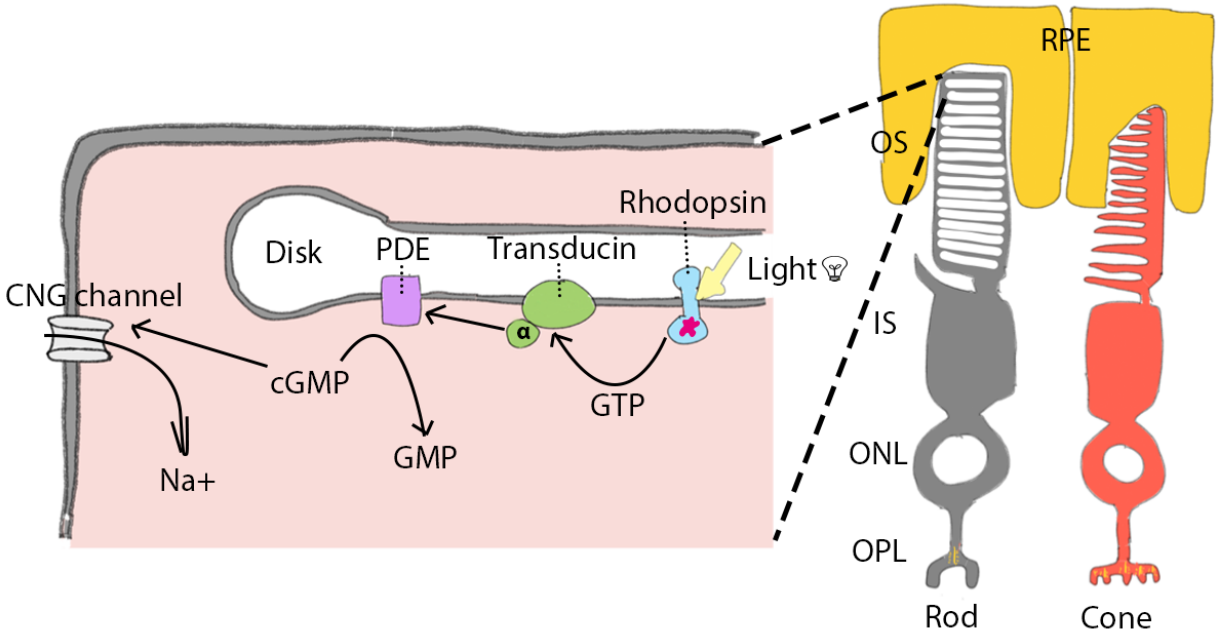

Figure 2: Schematic - Initial steps of phototransduction in rods

Schematic drawing of a rod and cone photoreceptor on the right. The left side demonstrates the light induced phototransduction in rods as described above. Retinal pigment epithelium (RPE), outer segments (OS), inner segments (IS), outer plexiform layer (OPL), guanosine triphosphate (GTP), phosphodiesterase (PDE), guanosine monophosphate (GMP), cyclic GMP (cGMP), cyclic nucleotide gated channel (CNGC).

1.2 Inherited retinal dystrophies

The heterogenous group of inherited retinal dystrophies (IRD) can cause partial to full loss of vision or other restrictions of sight. To this day, 289 genes have been identified in which mutations lead to many different vision disorders (https://web.sph.uth.edu/RetNet/, July 12, 2024). The general ability to diagnose the specific disease has increased after new methods in molecular genetics, like next-generation sequencing, have simplified and reduced the cost of diagnosis and enabled a more reliable prognosis (Georgiou et al., 2021). At present, no treatments are available for most of these diseases, and they can only be managed symptomatically and with aids for the blind.

This study focuses on retinitis pigmentosa (RP), which, with a prevalence of 1 in 3000 people, is the most common of these IRDs (Boughman et al., 1980). In the course of the disease the photoreceptor cells die. Especially the rods in the periphery degenerate, resulting in a secondary degeneration of the cones in the central regions. Similarly, in fundoscopy a degeneration with bone spicule-shaped dark pigment deposits along with retinal atrophy progressing from the periphery into the center can be observed. The macula will stay preserved until late stage RP, due to the high cone to rod ratio in the fovea, but presents a centripetal ring of depigmentation encircling itself in mid stages as shown in Figure 3**b** (Hamel, 2006). Since the rods enable monochromatic vision and the recognition of silhouettes under low light, symptoms such as night blindness and loss of peripheral vision develop in the early stages of RP (Figure 3**f**). Later, the secondary degeneration of peripheral cones leads to the phenomenon of tunnel vision. Eventually, with the loss of central cones as well, complete blindness sets in (Figure 3**d**). These symptoms are irreversible since photoreceptor cells, as postmitotic neurons, cannot be regenerated. Furthermore, there is currently no therapy that stops the progress of this disease or reverses the degeneration. The exact mechanisms of cell death are not yet fully understood, although mutations in 69 genes are known to be involved in different forms of RP. According to inheritance patterns, these disease genes can be subdivided into autosomal recessive (51 genes), autosomal dominant (23 genes) and dominant X-linked (2 genes) inheritance (https://web.sph.uth.edu/RetNet/, July 12, 2024). The genetic heterogeneity results in a broad range for the age of onset, symptoms, and speed of disease progression.

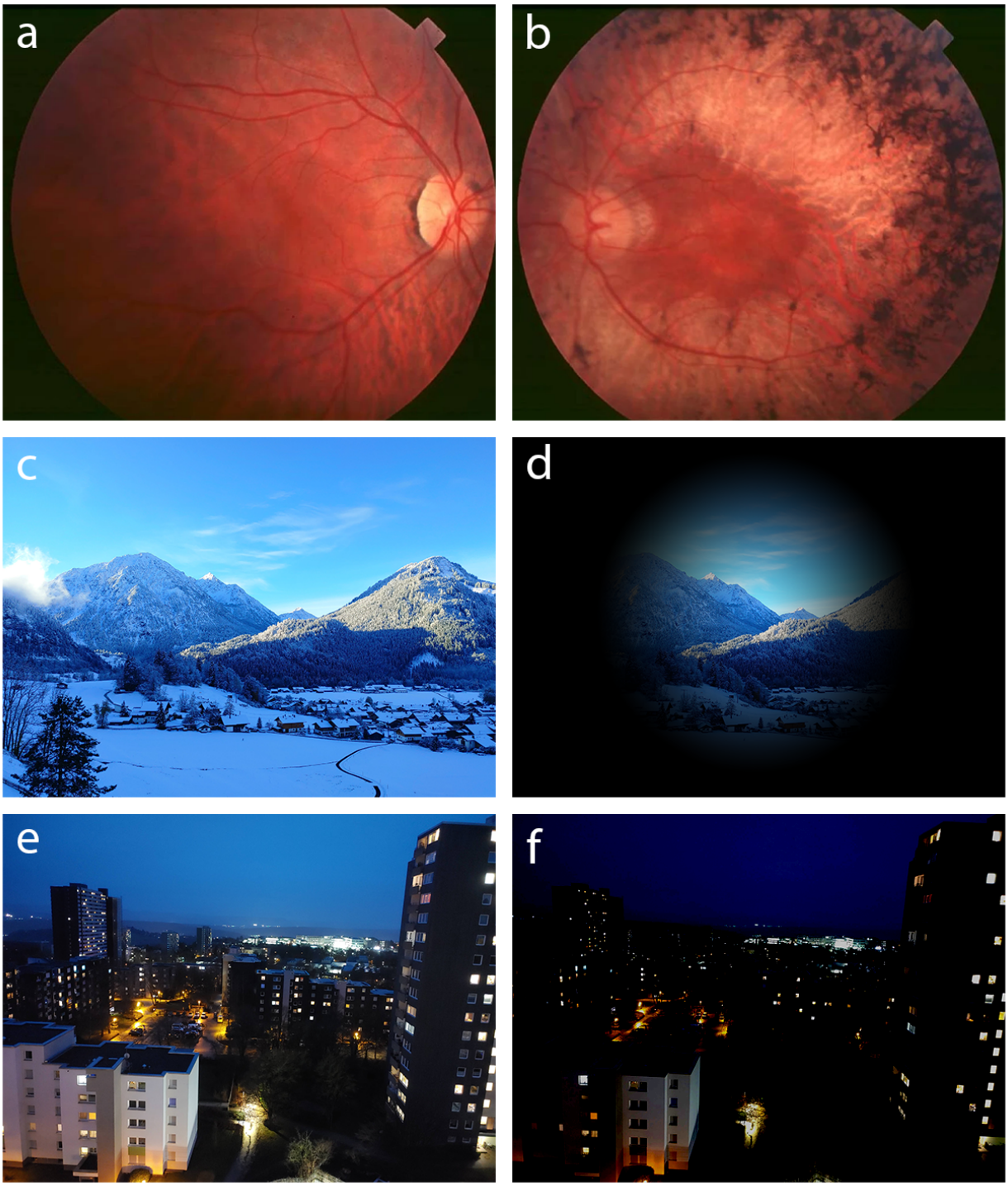

Figure 3: Comparison of the fundus, peripheral, and night vision between an unaffected individual and a Retinitis pigmentosa patient

*Fundoscopy picture of a healthy fundus **(a)**, fundoscopy picture in a mid-stage Retinitis pigmentosa (RP) patient **(b)**, unrestricted field of view **(c)**, visualization of tunnel vision of an advanced stage RP patient due to a degenerated retinal*

*periphery **(d)**, unrestricted night vision **(e)**, visualization of reduced recognition of silhouettes and night vision in RP patients **(f)**. Pictures **(a)** and **(b)** modified after (Hamel, 2006).*

1.2.1 Cell death pathway in RP

Although in the past it was often assumed that the loss of photoreceptors was triggered by an apoptotic cell death mechanism (Chang et al., 1993), newer research on photoreceptor degeneration in RP identified an alternative cell death mechanism that is not linked to either apoptotic or necrotic cell death. (Arango-Gonzalez et al., 2014). The proposed mechanism is shown in the schematic below (Figure 4). The mutations lead to a defect in phosphodiesterase 6 a or b, which is physiologically responsible for the degradation of cGMP to GMP. Due to the lack of degradation, cGMP accumulates and starts to trigger a cascade that ultimately leads to the degeneration of the rods (Farber and Lolley, 1974). In itself, cGMP is a ubiquitously occurring signaling molecule with many functions. However, a greatly increased cGMP concentration can over-activate the following two metabolic pathways:

Path 1 (left in Figure 4): The activity of protein kinase G increases, and the cascade first activates the enzyme histone deacetylase and then poly-ADP-ribose polymerase (PARP) (Paquet-Durand et al., 2009). The overproduction of poly-ADP-ribose by PARP results in the excessive consumption of the substrate NAD+, which is likely to trigger a breakdown in cellular energy metabolism. (Paquet-Durand et al., 2007).

Path 2 (right in Figure 4): The probability of the CNG channel opening is increased by the binding of cGMP, which in turn results in an increased influx of Ca^{2+} ions. (Paquet-Durand et al., 2011). The rising Ca^{2+} level lead to an increased activity of Ca^{2+}-dependent calpain proteases, which further degrade the cell proteolytically (Kulkarni et al., 2016). Both pathways are likely to contribute to cell degeneration and ultimately lead to cell death.

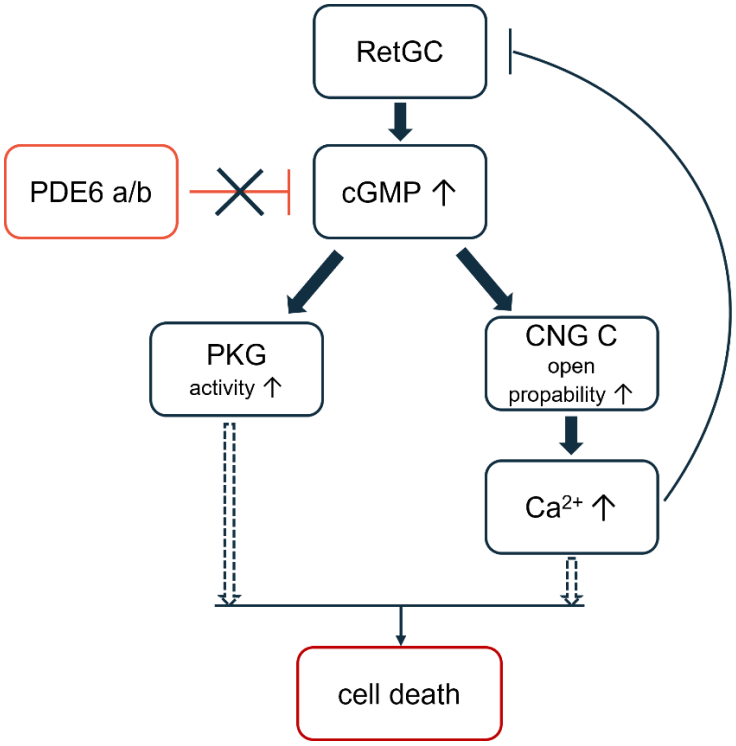

Figure 4: Cell death mechanism in RP with PDE6 mutation

The mutated enzyme photoreceptor phosphodiesterase 6 subunit a/b (PDE6 a/b) cannot break down cyclic guanosine monophosphate (cGMP), leading to accumulation in rod photoreceptors, activating different pathways that each lead to the death of the affected rod. The negative feedback loop mediated by calcium ions restricting retinal guanylyl cyclase (RetGC) activity is insufficient to stop this process. cGMP strongly activates protein kinase G (PKG), which then phosphorylates multiple targets, continuing the cascade until cell death occurs.

1.2.2 The *rd1* mouse model

Several animal models with different mutations exist for retinal degeneration and have been used to investigate the pathology of RP (Moshiri, 2021). One of these models is the *rd1* mouse. The severe early onset retinal degeneration observed in these animals leads to blindness and behavioral changes at a young age. Subsequent histological examinations have revealed that the animals' rodless retina is the cause of these changes (Keeler, 1924). This animal model is affected by homozygous mutations in the *Pde6b* gene by a nonsense mutation and a murine

viral insert (Bowes et al., 1990, Chang et al., 2002). The process of cells dying in the *rd1* animal model begins early and peaks at P13 (Sahaboglu et al., 2013). The degeneration leads to just 2% rods remaining at P17, with very few rods remaining at P47, and none left at P65 (Carter-Dawson et al., 1978). The *rd1* animal model in the *ex vivo* retinal explant culture system shows a similar degeneration process as *in vivo (Caffe et al., 1993)*.

The *rd1* animal model was in focus in different studies in search for a treatment option for RP. Axokine™ , a recombinant version of ciliary neurotrophic factor, was found to slow down progression in *rd1* animals after it was first tried as medication against amyotrophic lateral sclerosis (LaVail et al., 1998). During later studies researching Axokine™ to treat obesity, emergence of antibodies against the drug were found (Ettinger et al., 2003), leading to the discontinuation of its commercialization. Another promising compound was the calcium channel antagonist diltiazem, used in cardiology, which seemed to slow down cell death in *rd1* animals and rescue scotopic vision (Frasson et al., 1999). Subsequent studies on Ca^{2+}-pathway suppression showed ambiguous results, confirming (Read et al., 2002) and contradicting (Bush et al., 2000) Frasson's findings. This drew attention to the differences and incomparability of different pathogenic models and slowed down further research on this topic. The third example is more recent and proposes protein kinase G (PKG) as a target for neuroprotection in *rd1* (Paquet-Durand et al., 2009). Cell death is reduced by cyclic nucleotides analogues inhibiting the PKG pathway. Research on this subject is still ongoing (Tolone et al., 2023).

As stated above, extensive research on the *rd1* mouse model has already been performed. The early onset and rapid progression of this model allow for rapid experimental readouts and enable use in the relatively short time-frame of *ex vivo* culture systems, rendering the *rd1* an optimal choice for retinal explant cultivation. Finally, the currently discussed hypotheses on the underlying pathomechanisms of rod degeneration in *rd1* animals align with the mechanism of action of the drug MPA, which is the subject of this study. Taken together, the *rd1* animal model emerges as the optimal choice for investigating the mechanism of action of MPA.

1.3 Treatment approaches

To date there is only one drug approved for the treatment of IRD, which is the gene replacement therapy voretigene neparvovec (Luxturna®) for the gene *RPE65*. RPE65 mutations lead to an enzyme defect in the retinal pigment epithelium (RPE) (Koenekoop, 2008), which causes a very rapid Leber´s Congenital Amaurosis-type (LCA) retinal degeneration. Research in more slowly progressing RP is highly active with about 100 drugs in development of which approximately 50 % are Advanced Therapy Medicinal Products (ATMPs) (Cross et al., 2022). In contrast to gene therapies which may serve only small subsets of RP patients, cell replacement therapies and small molecule neuroprotection may be suitable for a broader number of IRDs and various forms of RP. In general, the goal of all such treatments is to rescue and maintain the photoreceptors. They are based on the prerequisite that the patient has not reached blindness, which presupposes that the diagnosis is made early. Additionally, gene therapies rely on thorough genetic testing and identification of the causative gene, as they aim to replace it. Cell-based therapies offer another option, but this approach is even less explored than the still relatively recent gene-focused therapies (Cross et al., 2022). Thus, conventional neuroprotective medication with a potentially broad utilization could be used to delay disease progression and could possibly be combined with gene-specific treatment approaches. However, neuroprotection requires a thorough understanding of the cell death inducing pathways. While the state of knowledge in this area has expanded significantly in the last decade, resulting in many new approaches, additional challenges must still be overcome to find a clinically useful medication (Scholl et al., 2016). For example, in RP where multiple mutations lead to elevated cGMP levels, the enzymes along this pathway may be potential drug or treatment targets. While substances inhibiting guanylyl cyclases (GCs) exist, they are not specific to the RetGC present in the retina. Due to the near ubiquitous expression of different GCs in other tissues, indiscriminate inhibition would likely lead to unpredictable side effects. Substances specifically targeting the retinal variant are currently not known (Dizhoor and Peshenko, 2021).

Additionally, due to the blood-retina barrier (BRB), many substances cannot reach their target. Injecting the active ingredient closely to the target could bypass the BRB, increase concentration and lower adverse systemic effects. For this to be viable, a suitable drug delivery system would be indispensable. This is a field of active research with promising strategies such as nanoparticles or liposomes which surround or bind to the active ingredient (Koo et al., 2012, Birngruber *et al*., 2014). Generally speaking, intravitreal injections are the method of choice for the administration of many drugs (*e.g.* anti-Vascular Endothelial Growth Factor (VEGF) antibodies) to the retina, with drug delivery systems that allow for a sustained release (Del Amo et al., 2017).

1.4 Inosine monophosphate dehydrogenase 1 as a target for retinal neuroprotection

As other studies have focused on downstream cGMP toxicity (Vighi et al., 2018, Christensen et al., 2023), I decided to assess the pathways upstream of cGMP and investigate for potential targets. At first glance RetGC may appear as an ideal target for such an approach. However, to our knowledge, no specific inhibitors are available to exclusively affect the retinal photoreceptors. As different GC isoforms are ubiquitously expressed in most cells, a broad inhibitory approach might provoke many unforeseeable side effects. By targeting upstream enzymes all downstream pathways leading to cell death by elevated cGMP levels are included, although the potential for adverse effects may rise with such a broader approach. Further up the pathway, the enzyme inosine monophosphate dehydrogenase 1 (IMPDH1) is responsible for catalyzing the rate limiting step from inosine monophosphate (IMP) to xanthosine monophosphate (XMP) with the reduction of nicotinamide adenine dinucleotide (NAD) to $NADH^{+}$ and thus also responsible for the *de-novo* synthesis of GTP as schematically shown in Figure 5 (Sakti et al., 2023, Hedstrom, 2009).

IMPDH is a highly conserved enzyme present in most organisms. Two different isoforms play important roles: IMPDH1 appears to be important for retinal

metabolism as it is expressed in the photoreceptors (Bowne et al., 2006, Kennan et al., 2003). IMPDH2 is important for a functioning immune system and cell proliferation through guanosine metabolism (Burrell and Kollman, 2022). In humans, mutations in the gene *IMPDH1* lead to Leber's Congenital Amaurosis 10 (OMIM #613837, LCA10) or autosomal dominant retinitis pigmentosa (OMIM #180105, adRP). Both are early onset diseases with rapid progression and early macular degeneration leading to a severe clinical picture at a young age (den Hollander et al., 2008, Bowne et al., 2002, Cleghorn et al., 2022). As with most retinal degenerations, their pathophysiology is not fully understood. Interestingly, a gain of function mutation in the *IMPDH1* gene, as seen in the *RP10* mouse model, also leads to photoreceptor degeneration although less severe and with slower progression (Bowne et al., 2006, Plana-Bonamaiso et al., 2020). With consideration of these points, the enzyme IMPDH1 shows potential as a drug target to reduce cGMP levels and consequently reduce rod cell death. This may be true for all disease-causing mutations that lead to an elevation of photoreceptor cGMP-levels.

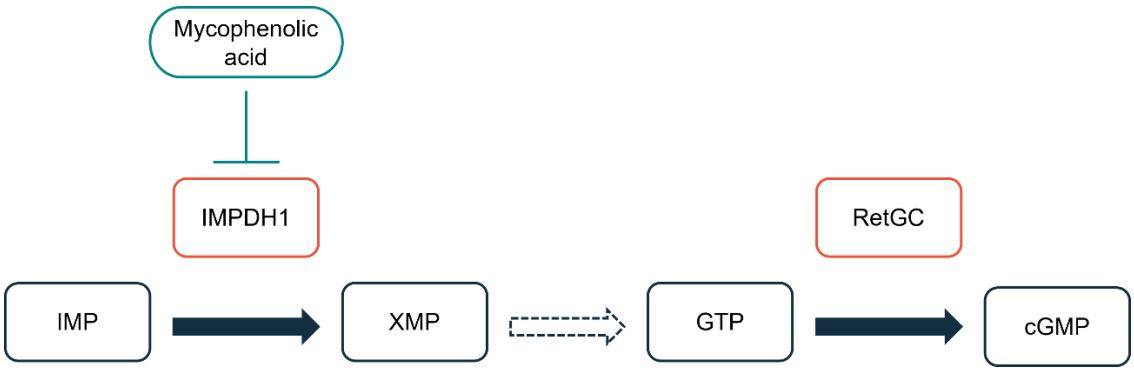

Figure 5: Mycophenolic acid targeting IMPDH1 and downstream pathway

The enzyme inosine monophosphate dehydrogenase 1 (IMPDH1) is the rate limiting step in the de-novo synthesis of guanine nucleotides by catalyzing the conversion of inosine monophosphate (IMP) to xanthosine monophosphate (XMP) and therefore influencing the absolute level of cyclic guanosine monophosphate (cGMP) per cell. Mycophenolic acid (MPA) can reversibly inhibit IMPDH1 leading to a reduced amount of available cGMP. The dotted arrow indicates omitted

intermediate steps in the pathway. Guanosine triphosphate (GTP), retinal guanylyl cyclase (RetGC).

1.5 Mycophenolic acid

Mycophenolic acid (MPA) potently and reversibly inhibits IMPDH1 and thus affects the rate-limiting step of GTP synthesis, the precursor of cGMP, reducing the absolute amount of cGMP in photoreceptor cells (Allison et al., 1993). MPA is an approved medication in the form of the prodrug mycophenolate mofetil for autoimmune diseases and for transplant patients as an immunosuppressive drug (Zwerner and Fiorentino, 2007, Jones et al., 2009). MPA is usually taken orally in tablet form under the names Myfortic® or CellCept® at a dose of up to 2 grams per day. In the case of transplant inpatients, it can also be applied intravenously. The blood-retina barrier can be passed by MPA, as it is electrically neutral and has a relatively low molecular weight ($C_{17}H_{20}O_6$, M_r = 320.34 g/mol). Other studies have found that MPA has further effects, which include antioxidant properties (Dalmarco et al., 2009), inhibition of leukocytes (Papadimitriou et al., 2003, He et al., 2011), attenuation of neuronal excitotoxic damages in the brain (Dehghani et al., 2003), inhibition of astrocyte and microglial inflammatory activation (Dehghani et al., 2010), and lastly the off-label use of MPA to treat ocular inflammation (Daniel et al., 2010).

In general, a treatment interfering upstream in a pathomechanism has a higher chance of side effects due to an increased amount of steps with possibly unknown influences. Due to this, treatment options usually try to target a mechanism as far downstream as possible to reduce side effects. Since increased cGMP can lead to cell death through more than one pathway, a downstream treatment might need to include multiple drugs, targeting multiple pathways. The systemic side effects of MPA are well known due to its common usage. They include gastrointestinal symptoms, bone marrow suppression and its consequences, *e.g.* infections and cytopenia. High concentrations in mice lead to severe side effects such as diarrhea and death (Yang et al., 2020).

1.6 Aims of the Study

As there is currently no treatment for the different forms of RP, the search for a compound that can prevent photoreceptor loss is of great interest for the field of ophthalmologic orphan diseases. The IMPDH1 inhibiting effects of MPA provide an opportunity to reduce photoreceptor cGMP levels and to exploit this for the development of a potential treatment for RP. This idea is reinforced by the approval of MPA as an immunosuppressant in post organ transplantation medication, where large doses of the substance are used, and extensive clinical data is available. Furthermore, initial positive results have already been obtained in *rd10* mice *in vivo* (Yang et al., 2020).

The main goal of this study was to use *ex vivo* organotypic retinal explants to assess the effects that MPA may have directly on retinal photoreceptors. To this end, the study addressed the following individual aims:

1. Evaluating the role of IMPDH1 and GC in the photoreceptor cGMP synthesis pathway.
2. Assessing the effect of MPA on WT and *rd1* rod and cone photoreceptors.
3. Creating a dose-response curve for MPA treatment to delineate an optimal dose for future *in vivo* studies.

2 Materials and methods

2.1 Materials

Different specialized devices, software, chemicals, and other materials were used for the experiments and evaluation of the results. Many of the chemicals mentioned were mixed according to protocols for the preparation of buffers, media, treatment, and staining, as seen in the following tables and listings.

Table 1: Devices and software used for experiments and analysis and their source

Software & Devices	Company
GraphPad Prism 9.5.1	GraphPad Software, Inc, La Jolla, CA, USA
Zeiss Axio Imager Z1 ApoTome Microscope	Zeiss Group, Oberkochen, Germany
Zeiss Axiovision software	Zeiss Group, Oberkochen, Germany
Microsoft Office	Microsoft Corporation, Redmond, WA, USA
Adobe Photoshop CC 2017	Adobe Systems Inc., San Jose, California U.S.
Thermo Scientific NX50 microtome	Thermo Scientific, Waltham, MA
Milli-Q® Lab Water Purification System	Merck KGaA, Darmstadt, Germany
DX-23 Autoclave	Systec, Wettenberg, Germany
Venticell Drying cabinet	MMM Medcenter, München, Germany
PIPETMAN, various sizes	Gilson Incorporated, Middleton, USA

Table 2: Information about various materials, substances and chemicals used in the experiments, and their respective sources

Chemicals & Materials	Company	Product number
Filtropur BT100, 1000 ml, 0.2 µm	Sarstedt Inc., Newton, NC, USA	83.3942.101
Cellstar Tubes, 50 ml	Greiner Bio-One, Kremsmünster, Austria	210261
Super Frost Slides	Emmendingen; R. Langenbrinck, Germany	02-0060/90
3M Comply Steam indicator Tape	3M Comply, Saint Paul, Minnesota, U.S.	1322-18MM
6-Well Culture Plates with Transwell Inserts	Corning Inc., Corning, New York, U.S.	3412

Tissue-Tek® O.C.T.™ Compound	Tissue-Tek, Leica, Bensheim, Germany	1418901035
A-PAP PEN Liquid-repellent Marker	Sigma-Aldrich Chemie GmbH, Taufkirchen, Germany	Z672542
Mounting medium: DAPI with Fluoroshield	Abcam, Cambridge, UK	ab104139
Basal R16 Medium	Invitrogen Life Technologies, Darmstadt, Germany	07490743
Bovine Serum Albumin (BSA)	Sigma-Aldrich Chemie GmbH, Taufkirchen, Germany	A7906
Transferrin	Sigma-Aldrich Chemie GmbH, Taufkirchen, Germany	T-8027
Progesterone	Sigma-Aldrich Chemie GmbH, Taufkirchen, Germany	P-8783
Insulin	Sigma-Aldrich Chemie GmbH, Taufkirchen, Germany	I-6634
Triiodothyronine (T3)	Sigma-Aldrich Chemie GmbH, Taufkirchen, Germany	T6397
Corticosterone	Sigma-Aldrich Chemie GmbH, Taufkirchen, Germany	862290
Thiamine HCl	Sigma-Aldrich Chemie GmbH, Taufkirchen, Germany	T1270
Vitamin B12	Sigma-Aldrich Chemie GmbH, Taufkirchen, Germany	V6629
(±)-α-Lipoic Acid (= Thioctic Acid)	Sigma-Aldrich Chemie GmbH, Taufkirchen, Germany	T1395
Retinol	Sigma-Aldrich Chemie GmbH, Taufkirchen, Germany	R7632
Retinyl acetate	Sigma-Aldrich Chemie GmbH, Taufkirchen, Germany	R7882
DL-Tocopherol	Sigma-Aldrich Chemie GmbH, Taufkirchen, Germany	T1539

Tocopheryl acetate	Sigma-Aldrich Chemie GmbH, Taufkirchen, Germany	1667701
Linoleic acid	Sigma-Aldrich Chemie GmbH, Taufkirchen, Germany	L1012
Linolenic acid	Sigma-Aldrich Chemie GmbH, Taufkirchen, Germany	L2376
L-Cysteine HCl	Sigma-Aldrich Chemie GmbH, Taufkirchen, Germany	C7477
Glutathione	Sigma-Aldrich Chemie GmbH, Taufkirchen, Germany	G6013
Sodium Pyruvate	Sigma-Aldrich Chemie GmbH, Taufkirchen, Germany	P3662
(+)-Na-L-ascorbat (Vit. C)	Sigma-Aldrich Chemie GmbH, Taufkirchen, Germany	A4034
Glutamine	Sigma-Aldrich Chemie GmbH, Taufkirchen, Germany	G8540
FBS / FCS	Sigma-Aldrich Chemie GmbH, Taufkirchen, Germany	F7524
TUNEL® assay (In Situ Cell Death Detection Kit)	Roche Diagnostics GmbH, Mannheim, Germany	12156792910
Acetic acid	Merck kGaA, Darmstadt, Germany	K43073263 202
Ethanol	Sigma-Aldrich Chemie GmbH, Taufkirchen, Germany	32205
Tween 20	Sigma-Aldrich Chemie GmbH, Taufkirchen, Germany	P7949
Paraformaldehyde (PFA)	Sigma-Aldrich Chemie GmbH, Taufkirchen, Germany	P 6148
Normal Donkey Serum	Abcam, Cambridge, UK	ab7475
Normal Goat Serum	Abcam, Cambridge, UK	ab7481

$NaH_2PO_4 \cdot H_2O$	Sigma-Aldrich Chemie GmbH, Taufkirchen, Germany	567549
NaH_2PO_4 (anhydrous)	Sigma-Aldrich Chemie GmbH, Taufkirchen, Germany	S5011
Tris	Sigma-Aldrich Chemie GmbH, Taufkirchen, Germany	154563
Proteinase K	Sigma-Aldrich Chemie GmbH, Taufkirchen, Germany	F7524
$NaSeO_3 \cdot 5\ H_20$	Sigma-Aldrich Chemie GmbH, Taufkirchen, Germany	S5261
$MnCl_2 \cdot 4\ H_20$	Sigma-Aldrich Chemie GmbH, Taufkirchen, Germany	S5761
$CuSO_2\ 5H_2O$	Sigma-Aldrich Chemie GmbH, Taufkirchen, Germany	C8027
Biotin	Sigma-Aldrich Chemie GmbH, Taufkirchen, Germany	B4639
Ethanolamine	Sigma-Aldrich Chemie GmbH, Taufkirchen, Germany	E0135
NaCl	Sigma-Aldrich Chemie GmbH, Taufkirchen, Germany	S9888
HCl	Sigma-Aldrich Chemie GmbH, Taufkirchen, Germany	H9892
NaOH	Merck kGaA, Darmstadt, Germany	Z0487239
Dimethyl sulfoxide	Sigma-Aldrich Chemie GmbH, Taufkirchen, Germany	8418
Mycophenolic acid ≥98%	Sigma-Aldrich Chemie GmbH, Taufkirchen, Germany	M5255

Media and Buffer solutions:

- PB (0.1 M) and PBS (0.01 M)
    1. Prepare 6.89 g $NaH_2PO_4 \cdot H_2O$ in 250 ml ultrapure water (0.2 M),

2. Prepare 14.19 g NaH_2PO_4 (anhydrous) in 500 ml ddH2O (0.2 M),
3. Add both solutions together to reach a pH of 7.4 (0.1 M PB),
4. Dilute 100 ml PB stock solution with 900 ml ultrapure water (ratio 1:10), for a concentration of 0.01 M,
5. Add 9 g of NaCl, carefully shake until dissolved to obtain 0.01 M PBS, store in a lidded bottle at 4 °C.

- TBS (50mM)
    1. Add 6 g of Tris into 900 ml ultrapure water,
    2. Adjust pH with 1 M HCl and NaOH until pH 7.6 is reached,
    3. Fill up with ultrapure water to 1 l,
    4. Add 9 g of NaCl, carefully shake until dissolved, store in a lidded bottle at 4 °C.
- Proteinase K:
    1. Dissolve the contents of the 25 mg vial in 250 µl ultrapure water,
    2. Dilute 225 µl of the solution in 18.5 ml basal Medium,
    3. Sterile filtration through 0.2 µm or smaller pores,
    4. Aliquot 1 ml into 2 ml Eppendorf Safe-Lock Tubes and store at 4 °C.

Stock solutions for Basal R16 Medium:

- $NaSeO_3$ 300 µM, $MnCl_2$ 50 µM, $CuSO_2$ 100 µM stock solution:
    1. Dissolve 7.9 mg of $NaSeO_3 \cdot 5\ H_2O$, 1.0 mg of $MnCl_2 \cdot 4\ H_2O$ and 2.5 mg of $CuSO_2 \cdot 5\ H_2O$ in 100 ml of ultrapure water and store.
- Biotin 0.1 mg/ml stock solution:
    1. Add 10 mg into 9,8 ml ultrapure water,
    2. Add 0.1 ml 1N NaOH (pH 10-12),
    3. heat to +35º C and stir for approximately 10 minutes until biotin is dissolved,
    4. Neutralize with 0.1 ml 1N HCl,
    5. Add 1 ml of this to 9 ml ultrapure water and store.
- Ethanolamine 1 mg/ml stock solution:
    1. Add 0.01 ml of ethanolamine to 10 ml distilled H_2O,
    2. Filter and store.

Stock solutions for Complete Medium (sterile conditions or sterile filtration):

- BSA (10%):

1. Add 2 g BSA to 100 ml ultrapure water,
2. Stir for ~2 hours until dissolved and store.

- Transferrin (10 mg/ml):
    1. Add 25 mg to 2.5 ml of ultrapure water,
    2. Filter and store.
- Progesterone (6.3 µg/ml):
    1. Add 2.52 mg progesterone to 4 ml pure ethanol, stir and filter,
    2. Add 0.1 ml of the solution to 9.9 ml 0,1% sterile albumin and store.
- Insulin (2 mg/ml):
    1. Coat the inside of a glass beaker with 0.1% BSA,
    2. Add 10 ml ultrapure water, 20 mg of insulin and 2 drops of HCl to the beaker, filter, and store.
- Triiodothyronine (T3) (2 µg/ml):
    1. Add 2 mg of T3 to 0.1 ml 1N NaOH and 9.9 ml 0.01% albumin and filter,
    2. Add 0,1 ml of the solution to 9.9 ml sterile 0.01% albumin and store.
- Corticosterone (20 µg/ml):
    1. Add 8 mg of corticosterone to 4 ml pure ethanol and filter,
    2. Of this, add 0.1 ml to 9.9 ml 0.1% BSA and store.
- Thiamine HCl (Vit. B1) (2.77 mg/ml):
    1. Add 27.7 mg thiamine HCl to 10 ml ultrapure water,
    2. Filter and store.
- Vit. B12 (0.31 mg/ml):
    1. Add 3.1 mg vitamin B12 to 10 ml ultrapure water,
    2. Filter and store.
- (±)-α-Lipoic Acid (= thioctic acid) (45 µg/ml):
    1. Add 45 mg lipoic acid to 10 ml pure ethanol and filter,
    2. Of this, add 0.1 ml to 9.9 ml sterile albumin and store.
- Retinol / retinyl acetate (0.05 mg/ml, 0.05 mg/ml):
    1. Add 20 mg of both to 2 ml pure ethanol and filter,
    2. Add 0.05 ml of the solution to 9.95 ml 0,1% sterile albumin and store.
- DL-Tocopherol / tocopheryl acetate (0.5 mg/ml, 0.5 mg/ml):
    1. Add 200 mg of both to 2 ml pure ethanol and filter,
    2. Add 0.1 ml of this to 9.9 ml 10% sterile albumin,
    3. Shake for 5 minutes (solution will clear up after >24 hours), store.

- Linoleic acid / linolenic acid (0.5 mg/ml, 0.5 mg/ml):
    1. Add 111 µl linoleic acid and 108 µl linolenic acid to 1.781 ml pure ethanol and filter,
    2. Add 0.1 ml of this solution to 9.9 ml 10% sterile albumin,
    3. Shake for 5 minutes (solution will clear up after >24 hours), store.
- L-cysteine HCl (7.07 mg/ml):
    1. Add 70.9 mg L-cysteine HCl to 10 ml ultrapure water,
    2. Filter and store.
- Glutathione (1 mg/ml):
    1. Add 10 mg glutathione to 10 ml ultrapure water,
    2. Filter and store.
- Sodium pyruvate (50 mg/ml):
    1. Add 500 mg sodium pyruvate to 10 ml ultrapure water,
    2. Filter and store.
- Glutamine / vitamin C (2.5 mg/ml, 10 mg/ml):
    1. Add 25 mg of glutamine and 100 mg of vit. C to 10 ml ultrapure water,
    2. Filter and store.

2.2 Animals

Animals were provided by the animal facility of the Ophthalmic Research Institute of the University Tübingen. All animals were kept in a 12h day/night cycle and had *ad libitum* access to feed and water. The test animals were selected without consideration of their gender. For *ex vivo* retinal explant cultures, animal models of the C3H strain were used, these included C3H *Pde6b* $^{rd1/rd1}$ (*rd1*) and congenic C3H *Pde6b* $^{+/+}$ (wild-type; WT) animals (Sanyal and Bal, 1973). The same animals, at ages between P11 to P30 were used *in vivo* for different staining procedures. The procedures done on or with animals were authorized by the Tübingen University committee on animal protection and were carried out in compliance with the German animal protection act, as well as the guidelines for the use of animals in vision research by the association for research in vision and ophthalmology (ARVO). Efforts were made to reduce the number of animals used and no experiments were carried out on live animals.

2.3 Histology

The preparation of the organotypic retinal explant cultures begins with enucleation of the eyeballs from the sacrificed animal. The eyeballs were incubated at 37°C in protein kinase K to break the cell connection between outer layers and the RPE to keep it in place and connected to the retina during preparation. The retina was removed stereoscopically by slowly tearing the sclera and choroid off the eyeball. It was then cut into a clover shape and applied to the inserts with membranes of a 6-well-culture plate. The retinas were incubated at 37 °C, 5% CO_2 and the chemically defined serum free culture medium (complete R16 medium) was replaced regularly. After an adaptation phase of 2 days, the retinas were treated with active substances for 4 days until P11, all mediums were prepared after (Vighi et al., 2018, Belhadj et al., 2020). The entire process needed to be done under sterile conditions to avoid contamination of the cultures

The following substances/media needed to be prefabricated under sterile conditions before starting the process of retinal explant culture:

Basal R16 Medium (BM):

1. Dissolve one vial of powdered medium in 500 ml purified water,
2. Add 2.73 g $NaHCO_{3,}$
3. Add 0.1 ml 300 µM NaSeO / 50 µM $MnCl_2$ / 100µM $CuSO_2$ stock solution,
4. Add 1.0 ml Biotin 0,1 mg/ml,
5. Add 1.0 ml Ethanolamine 1 mg/ml,
6. Add 1.0 ml CDP Choline,
7. Add 800 ml ultrapure water,
8. Sterile filtration through 0.2 µm or smaller pores,
9. Aliquot into sterile 50 ml tubes.

Complete Medium (CM):

1. 40 ml of Basal R16 Medium into a sterile 50 ml tube,
2. 2.5 ml BSA,
3. 50 µl Transferrin,
4. 50 µl Progesterone,

5. 50 µl Insulin,
6. 50 µl T3,
7. 50 µl Corticosterone,
8. 50 µl Thiamine HCL,
9. 50 µl Vitamin B12,
10. 100 µl (±)-α-Lipoic Acid,
11. 100 µl Retinol / retinyl acetate,
12. 100 µl DL-Tocopherol / Tocopheryl acetate,
13. 100 µl Linoleic acid / linolenic acid,
14. 50 µl L-cysteine HCl,
15. 50 µl Glutathione,
16. 50 µl Na-Pyruvate,
17. 500 µl Glutamine / Vitamin C,
18. Fill up to 50 ml with autoclaved ultrapure water.

The whole procedure was carried out inside a laminar airflow hood. Personal protection equipment like gloves, mask, hair cap and coat are worn. Tools, pipettes, and containers were autoclaved, and sterile-packed or sterile-packed single-use materials were utilized. The autoclaved toolbox contents were two straight and one angled jeweler's forceps with pointy tips, one curved mini scissors, one regular small tweezer, and a small tissue spoon. The work surface of the laminar airflow hood was wiped with 70% ethanol. All sterile products were opened inside the hood. The proteinase K was preheated in an incubator to 37 °C. Two petri dishes with BM and one petri dish with FCS added to BM in a one to four ratio (20%) were prepared. Generally, the less time spent extracting the retina from the animal, transferring it to the incubator and the less amount of physical manipulation of the retina, the less damage is done and the better the subsequent results will be.

Retinal explant protocol (Belhadj et al., 2020):

1. Sacrifice the animal using an appropriate method for the age (P5 mice are decapitated),
2. Wrap a 70% ethanol-soaked napkin around the head,
3. Extract eyes under a stereoscope and incubate in BM at RT for 5 minutes,

4. Relocate the eyes into prepared PK solution an incubate at 37 °C with agitation for 15 minutes,
5. Immerse the eyes into prepared FCS solution to deactivate PK for 5 minutes,
6. Transfer the eyes into another petri dish with BM for washing,
7. Keep the eye from moving by holding the optical nerve with forceps,
8. Cut into the cornea and tear away the sclera without damaging the layers below,
9. Pull the lens out of the eyecup,
10. Cut the eyecup into a clover shape with 4 cuts so that the retina can lay flat,
11. Use a wide cut 1 ml pipette to transfer the retina onto a membrane insert of a 6-well plate,
12. Add 1.2 ml complete medium to the well and cover with plate lid,
13. Incubate until medium change in HERACELL 150i CO^2 Incubator,
14. Change medium after 48 hours,
15. Keep discarded medium in sterile tubes and incubate to check for possible contamination,
16. All reusable tools are repackaged after cleaning, closed with steam indicator tape, autoclaved, and kept in a drying cabinet until dry.

After the explant treatment were finished, the retinas were removed from the culture inserts. The retinas were fixed with 4% PFA and infiltrated with increasing concentrations of sucrose (10%, 20%, 30%) for cryoprotection. The added substances were removed after every step. Before shock freezing with liquid nitrogen, they were embedded in embedding compound. Finally, 12 µm thick sections were cut at the Thermo Scientific NX50 microtome and stored at -20 °C on Super Frost Plus slides until further processing. The following substances needed to be prefabricated before the fixation step:

- PFA 4%:
    1. Heat 150 ml of PB in a glass beaker to ~60 °C,
    2. Add 12 g of PFA to the glass beaker for 45 minutes,
    3. Fill up with PB until solution clears but stay below 280 ml,
    4. Let cool until RT, then add NaOH until pH of 7.4 is reached,
    5. Fill up to 300 ml with PB and check that pH is at ~6.9.
- Sucrose solutions:
    1. 10%: Dissolve 20 g of sucrose in 200 ml PB.

2. 20%: Dissolve 40 g of sucrose in 200 ml PB.
3. 30%: Dissolve 60 g of sucrose in 200 ml PB.

Protocol and substances used:

- Fixation in 4% PFA for 45 minutes (explants still in 6 well inserts)
- Wash the fixed explants with PBS 3 times each 5 minutes,
- Cryoprotection with sucrose
    1. 10% for 10 minutes,
    2. 20% for 20 minutes,
    3. 30% overnight at 4 °C.
- Embedding:
    1. Fill embedding medium into molds made from aluminum foil,
    2. Cut explant from the culture insert and transfer into embedding medium,
    3. Align the explant in the medium one side of the form and mark (remove any build up bubbles)
    4. Add liquid nitrogen to a Styrofoam box up to the upper limit of the metal block inside and put the molds on top to freeze.
- Cutting:
    1. The aluminum foil is removed inside the cold chamber of the cryotome,
    2. Using embedding medium, the block is melded to the block holder with respect to the explant's alignment,
    3. 50 µm cuts are made until the explants tissue is visible,
    4. 8 cuts of 12 µm thickness are mounted on Super Frost slides,
    5. The slides are dried at 37 °C for 30 minutes before storing at -20 °C in slide containers.

In rare cases, the explants were discontinued and ultimately discarded. The exclusion criteria used were medium discoloration, visible bacterial contamination and retinal destruction or artifacts visible in the microscopic examination which led to the quantitative evaluation being impossible or unrepresentative. Inconsistencies in the explant preparation and other unexpected problems could be the cause for the unsuitability.

2.4 Mycophenolic acid treatment

Two stock solutions with a concentration of 5 µM and 21 µM were created from mycophenolic acid by dissolving the powder in Dimethyl Sulfoxide (DMSO). The solutions were filtered sterile through 0.2 µm or smaller pores, aliquoted and frozen at -20 °C until use. Varying amounts of MPA solved in DMSO were added to the complete medium used for culturing the retina explants to reach the desired concentration. The prepared medium was then added to the explants at P7 and P9 after discarding the previously used medium. The treatment time was 48 hours after each medium change and added up to four days in total. *Ex vivo* explants are able to show the intended effects of MPA without regard to side effects thus allowing precise control of the substance concentration. Instead of the prodrugs used in human treatment, for our experiments the active metabolite MPA was chosen as metabolic transformations are not necessary due to direct application. MPA is not soluble in water, so to be able to add it to the treatment medium, DMSO was used as a solvent. DMSO is a popular and common solvent for substances in cell and organ culture. Six different concentrations of MPA between one and 1000 µM MPA were added to treat the explants with. A common dose approved in humans as antirejection medication for transplant patients is one gram per day orally of MMF, mycophenolate mofetil, a prodrug of MPA with improved oral availability, which results in a maximum fluid concentration of about 25 mg/L in healthy individuals (Bullingham et al., 1998), translating to a concentration of 78 µM. The doses tested were extended by two log units below the base dose at 1 µM, 10 µM and 40 µM MPA and by 1.5 log units above the base dose at 250 µM and 1000 µM MPA. This was done to establish a complete dose-response curve, possibly covering the non-effective to toxic range.

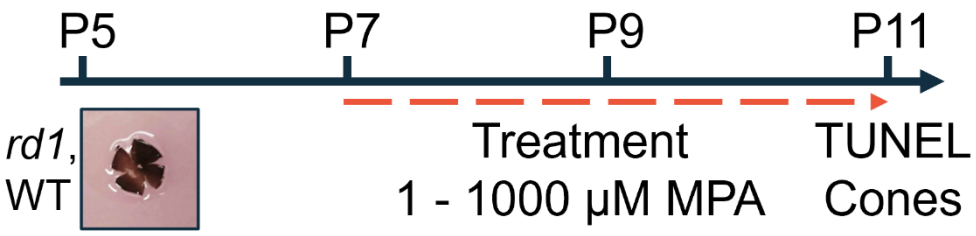

Figure 6: Workflow for explants, treatment and read-out

Wild-type (WT) and rd1 animals were sacrificed and their retinas prepared for organotypic retinal explant culture at postnatal day 5 (P5). At P7 and P9 the medium was changed, and treatment or controls added. At P11 cultivation was stopped, the explants fixed, embedded, and further processed for TdT-mediated dUTP-biotin nick end labeling (TUNEL), which labels cell death, and cone staining. Mycophenolic acid (MPA).

2.5 TUNEL assay

The TdT-mediated dUTP-biotin nick end labeling (TUNEL) method detects DNA components of cells in the process of dying regardless of the causative mechanism, and generates a fluorescent signal in the process (Gavrieli et al., 1992, Grasl-Kraupp et al., 1995). The duration of the staining requires about two days but depends on the TUNEL-Kit used. The cryosections must already be fixed to be processed further for a successful staining. The following mixtures and solutions must be prepared before the staining process:

- Alcohol-acetic mixture:
    1. 49 parts of 70% ethanol (EtHO),
    2. 9 parts 30% Acetic acid,
    3. 21 parts purified water.
- Proteinase K Solution:
    1. 42 ml of 50mM TBS,
    2. 6 µl of Proteinase K.
- TUNEL Blocking Solution:
    1. 33.75 ml PBS,
    2. 5 ml 10% NGS,

3. 5 ml 1% BSA,
4. 1250 µl Fish Gelatin.

- TUNEL Kit:
    1. 50 ml enzyme,
    2. 450 ml labeling solution,
    3. 500 ml TUNEL Blocking solution.

Protocol and substances used:

1. Switch on the incubator and set temperature to 37 °C,
2. Surround tissue with liquid-repellent and dry cryosections at 37 ° C,
3. Incubate Tris-PK solution at 37 °C until warmed,
4. Wash slides with PBS for 10 minutes,
5. Add Tris-PK solution to the slides and incubate for 5 minutes,
6. Wash slides with TBS for 5 minutes,
7. Apply Alcohol Acetic mixture (-20 °C) to the slides for 5 minutes,
8. Wash the slides with TBS 3 times each for 5 minutes,
9. Apply 200 µl TUNEL BS to each slide and incubate at RT for 1 hour,
10. Apply TUNEL-Kit mixture and incubate over night at 4 °C,
11. Wash the slides with PBS 3 times each for 5 minutes,
12. Add 4’,6-diamidino-2-phenylindole (DAPI) counterstaining and VECTASHIELD® Antifade Mounting Medium,
13. Add cover glass to the slides, store in fridge or start microscopy.

2.6 Immunofluorescence staining

A primary antibody is added to the cryosections, which binds to the corresponding molecule of interest. A secondary wavelength specific fluorophore-conjugated antibody then binds to the primary antibody, which is excited by filtered light and causes fluorescence, which can be observed under the microscope (Arango-Gonzalez et al., 2014). The immunostainings take two days until microscopy can be performed. Staining was complemented by a DAPI counterstaining and the application of VECTASHIELD® Antifade Mounting Medium to prolong the immunofluorescent signal. The following solutions need to be prepared before the staining process:

- PBST 0,3%:
    1. Add 499.94 ml PBS to a 0,5 l lidded bottle,
    2. Add 60 µl Triton X-100 detergent,
    3. Slowly stir, close lid and store at 4 °C.

Protocol and substances used:

1. Switch on the incubator and set temperature to 37 °C,
2. Prepare BS: add 10% (in conc.) 2° AB animal hosts serum and 1% (in conc.) BSA to 0.3% PBST, 400 µl per slide,
3. Surround tissue with liquid-repellent and dry cryosections at 37 °C,
4. Wash the slides with PBS for 10 minutes,
5. Apply ~150-200 µl Blocking Solution to each slide,
6. Incubate the slides at RT for 1 hour,
7. Dilute 1° AB in BS as per necessary dilution factor and apply to slides,
8. Incubate at 4 °C over night or for 1-2 hours at RT,
9. Wash the slides with PBS 3 times each 10 minutes,
10. Dilute 2° AB in PBS as per necessary dilution factor and apply to slides,
11. Incubate for 1 hour at RT in the dark,
12. Wash with PBS 3 times each 10 minutes,
13. Add DAPI counterstaining and VECTASHIELD® Antifade Mounting Medium,
14. Add cover glass to the slides and store or start microscopy.

The distribution of IMPDH1 in the retina was shown via a polyclonal antibody. Another monoclonal antibody was tried as well, but signaled artifacts and stained blood vessels without staining any part of the neuroretina. Particulate guanylate cyclase E (PGCE) is a guanylyl cyclase subunit. While the subunit is only present in rodents, the location of GC is expressed in the same structures in humans as in mice. Anti-peanut agglutinin (anti-PNA) is a fluorescein-conjugated antibody and stains the inner and outer segments of cones, it was used for quantification purposes. Anti-cone arrestin was also tested for quantification, but displayed artifacts and was difficult to count in retinal explant staining, likely because of the early post-natal age of the retina and the still incomplete differentiation/maturation of cones. Therefore, the more reliable peanut agglutinin (PNA) staining was used for cone quantification. To further specify the location of IMPDH1 stained signals, a Colocalization with anti-glutamine synthetase was performed. Anti-PGCE was

colocalized with anti-rhodopsin. Anti-cGMP was tried several times on retinal explant culture and normal sections, these could not be evaluated due to low signal intensity.

Table 3: Primary antibodies and where they were sourced

Primary Antibody	Host	Dilution	Company	Serial Number
Anti-IMPDH1 polyclonal	Rabbit	1:100	Abcam	ab33039
Anti-IMPDH1 monoclonal	Mouse	1:250	Merck Millipore	MABN291
Anti-PGCE	Rabbit	1:100	FabGennix	PGCE-501AP
Anti-cone arrestin	Rabbit	1:500	EMD Millipore	AB15282
Anti-PNA, fluorescein conjugated (514-521 nm, green)	-	1:200	Vector Laboratories	FL-1071
Anti-glutamine synthetase	Mouse	1:1000	Merck Millipore	MAB302
Anti-rhodopsin	Mouse	1:350	Merck Millipore	MAB5316
Anti-cGMP	Sheep	1:500	Harry W.M. Steinbusch, Maastricht University, Netherlands	-

Table 4: Secondary antibodies and where they were sourced

Secondary Antibody	Host	Dilution	Source	Dye (nm)
Anti-rabbit	Goat	1:350-500	Molecular Probes, A11034	AF 488 (green)
Anti-mouse	Goat	1:350-500	Molecular Probes, A11031	AF 568 (red)
Anti-rabbit	Donkey	1:350-500	Invitrogen, 10042	AF 568 (red)
Anti-mouse	Goat	1:500	Molecular Probes, A21424	AF 555 (red)
Anti-sheep	Donkey	1:350	Invitrogen, 11015	AF 488 (green)

2.7 Microscopy

Morphological observations and fluorescence microscopy were performed on a Zeiss Axion Imager Z1 ApoTome Microscope equipped with a Zeiss Axiocam digital camera and an APOCHROMAT objective with x20 or up to x63 magnification. The images are acquired, processed, edited, and archived with Zeiss Axiovision 4.2 software. For quantification, single layer pictures were taken, while for presentation and structure analysis layered Z-Stacks were created. For the latter the exposure time was regulated according to the intensity and type of staining and was between 0.03 seconds and 1.5 seconds. Maximum intensity projection was used on the latter, after which the pictures were saved as .tiff files. These were cut to size, rotated, composited, and labelled in Adobe Photoshop CC 2017.

2.8 Statistical Analysis

The TUNEL positive labeled cell cores were manually counted on at least 5 images with fixed black (100) and white (1000) values, the gamma value remained

unchanged at 1.0. The total number of cells in the outer nuclear layer (ONL) was calculated by dividing the ONL surface area through the average cell size of 16 µm². The average is calculated by measuring the ONL cells of retinal explants in multiple layers of ZEN microscopy. This number is divided by the amount of counted TUNEL positive cells in the marked area to determine the percentage of TUNEL positive cells.

To acquire the photoreceptor row count of the ONL, 9 vertical lines on 3 pictures per explant were set on the outer plexiform layer through the ONL. The DAPI-stained cell bodies were counted manually along the inserted lines.

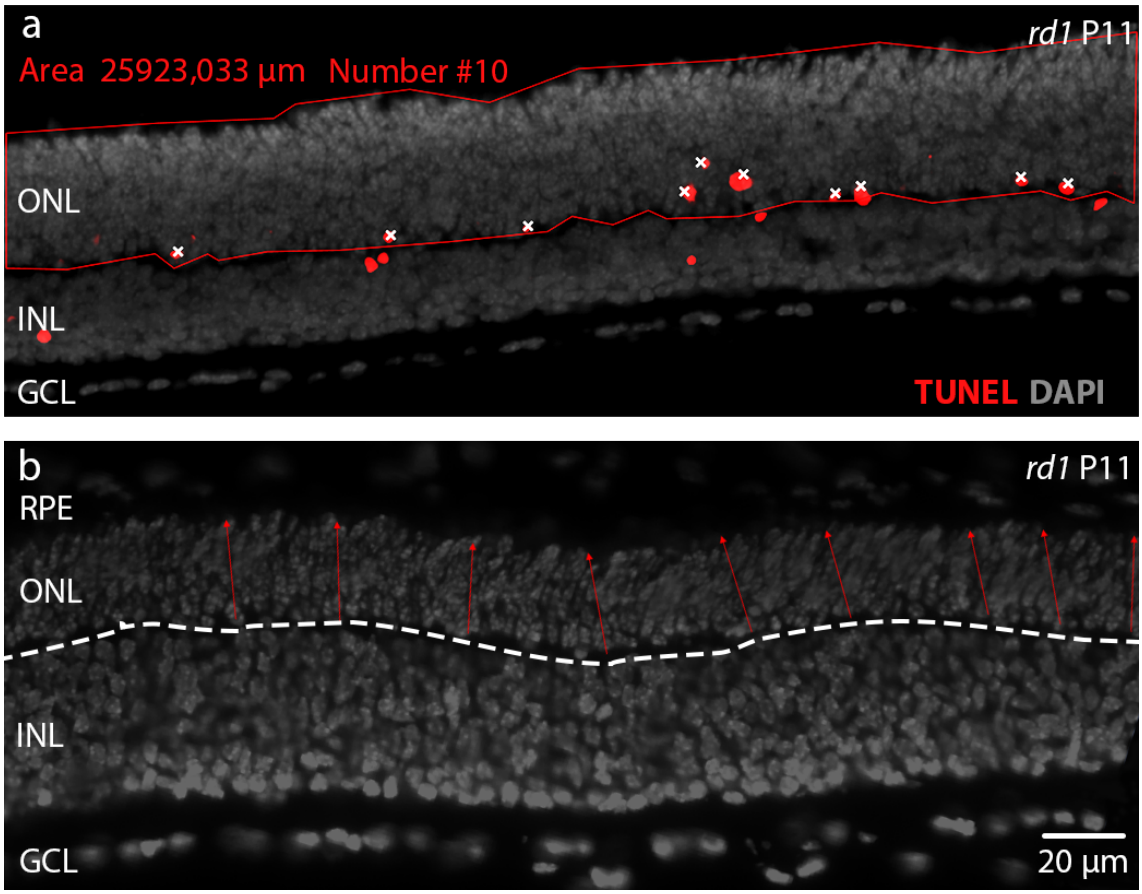

Figure 7: Demonstration of cell death percentage and ONL photoreceptor row data acquisition process

Microscopy picture of a treated rd1 explant, the ONL is outlined to determine ONL area, red signals show TUNEL positive cells and counting is performed by marking the m with a white cross ***(a)****. Microscopy picture of a treated rd1 explant****,*** *DAPI-stained cell nuclei were counted along the lines drawn vertically on the outer*

plexiform layer (dashed white line) ***(b)****. Outer nuclear layer (ONL), inner nuclear layer (INL), ganglion cell layer (GCL), retinal pigment epithelium (RPE), TdT-mediated dUTP-biotin nick end labeling (TUNEL, red), 4',6-diamidino-2-phenylindole (DAPI, grey), postnatal day (P).*

For cone photoreceptor quantification the PNA-stained segments were manually counted along with the number of positive cells along the segmental layer of the retina. For counting, varying black and white values were used to take differences of the signal intensity into account, gamma value remained unchanged at 1.0. The number of detected cones was counted per 100 µm length for comparison between explants.

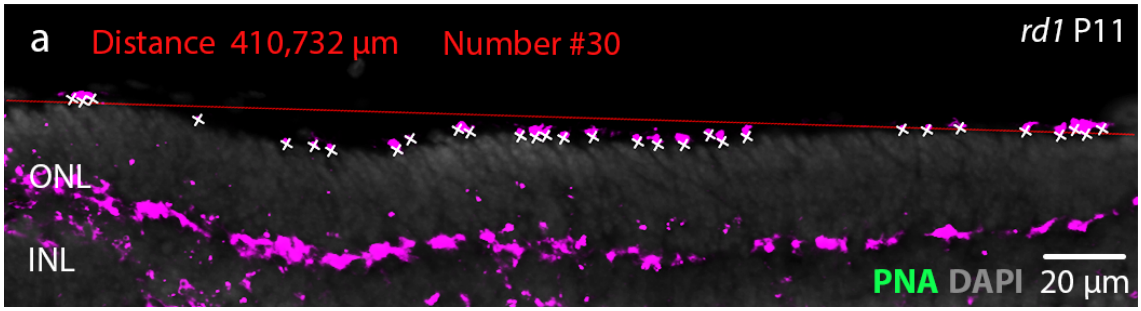

Figure 8: Demonstration of cone photoreceptor data acquisition process

Microscopy picture of a treated rd1 explant, a line along the ONL is drawn to determine distance, the violet dots on the ONL that indicate Peanut agglutinin (PNA, violet)*-stained cone photoreceptor outer segments are counted (****a****). Outer nuclear layer (ONL), inner nuclear layer (INL), 4',6-diamidino-2-phenylindole (DAPI, grey), postnatal day (P).*

The experimental groups data was first collected and averaged. The complete datasets were later transferred for statistical analysis and creation of graphs and curves. Depending on the type of datasets, different tests were used depending on the distribution and deviation of data points. These included unpaired t-tests for two group comparison, One-way ANOVAs (Brown-Forsythe, Bartlett's) or Kruskal-Wallis tests for more than two groups. For multiple comparisons Tukey's,

Dunnett's or Dunn's tests were used. Stages of significance were as follows: n.s., * = $p < 0.05$, ** = $p < 0.01$, *** = $p < 0.005$, **** = $p < 0.001$.

3 Results

3.1 IMPDH1 is expressed in photoreceptors

The first goal of this thesis was to demonstrate the expression of the enzymes relevant for cGMP signaling in photoreceptors. IMPDH1 is the target for MPA treatment and catalyzes the first, rate-limiting in the synthetic pathway leading up the generation of cGMP. IMPDH1 showed signals in different parts of the neuroretina: the retinal ganglion cells in the GCL, different cell types in the INL, neuronal synapses in the OPL and branches surrounding the DAPI stained cell cores of the ONL. The strongest signal could be detected in the photoreceptor segments, where IMPDH1 expression was observed in short parallel strokes, directly situated on the ONL. (Figure 9**a**, **b, c**). Between the two signals some infrequent offshoots reached slightly into the outer segment part, suggestive of the cilium region connecting the inner and outer segments. While IMPDH1 was seen as an area staining in the lower magnifications, in Figure 9**d, e** a greater magnification is shown (x63, immersion oil) where the IMPDH1 immunofluorescent signal was made up of many small clots. This is indicative of the filament structure in which the enzyme is usually present (Cleghorn et al., 2022).These mesoscale filament structures of IMPDH1 can form in mammalian cells with high GTP throughput (Keppeke et al., 2018, Aughey and Liu, 2015, Chang et al., 2015, Liu, 2010, Agrahari et al., 2016). The P11 *rd1* stainings of IMPDH1 showed essentially the same results as in the WT, with the distinction that the rod photoreceptors already began to die off and the ONL started to lose thickness. When only a monolayer of photoreceptor cells was left in older *rd1* animals, the enzyme´s signal in the inner segments was lost as well (Figure 9 **f, g, h, i**). The colocalization with rhodopsin, which was exclusively present in the outer segments, restricted IMPDH1 expression strictly into the photoreceptors inner segments (Figure 10) (Alpern et al., 1987).

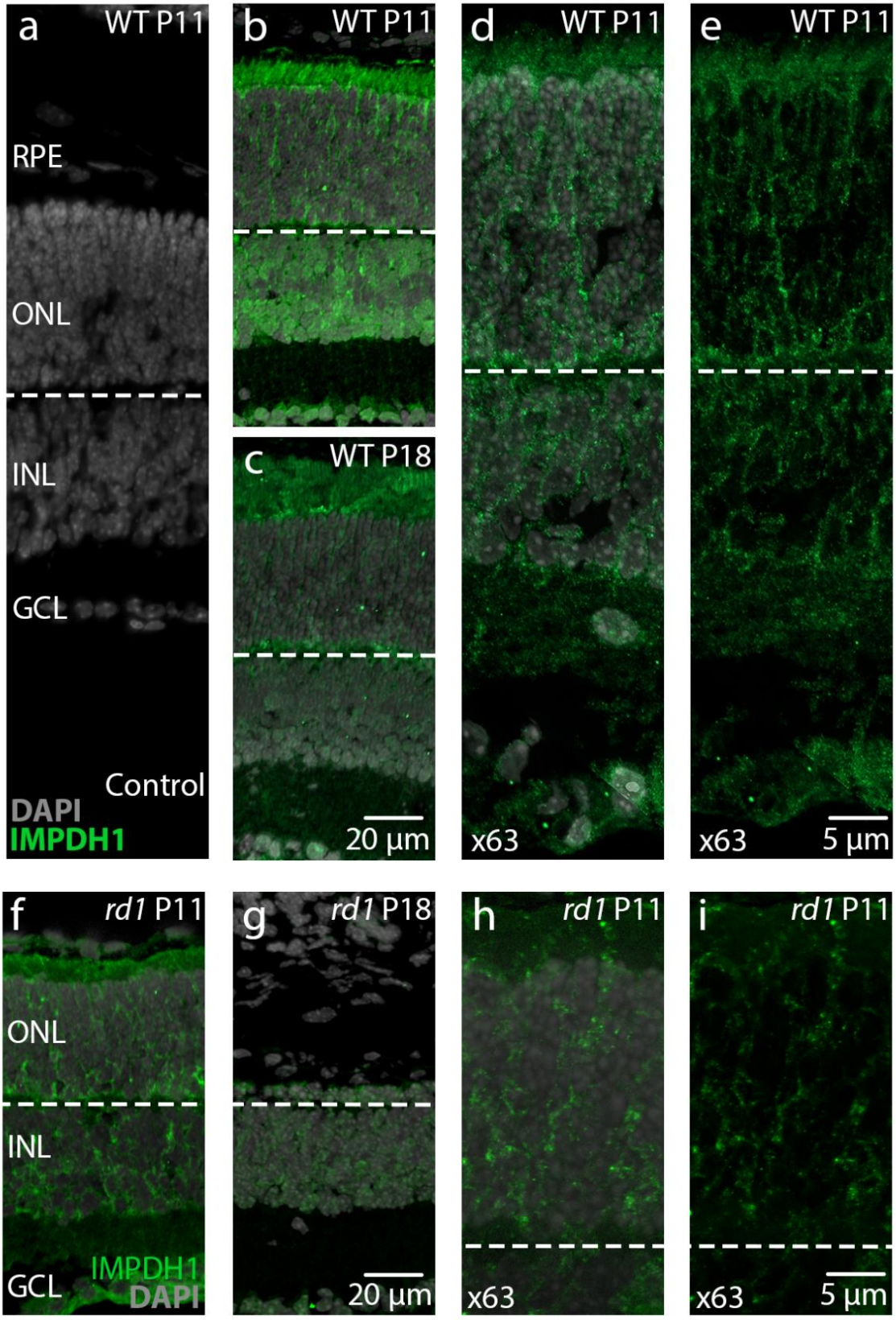

Figure 9: Expression of IMPDH1 in wild-type and rd1 retina

*Retinal in vivo cross-sections of wild-type (WT) animals were immunostained to visualize inosine monophosphate dehydrogenase 1 (*IMPDH1*, green) expressions patterns. 4',6-diamidino-2-phenylindole (DAPI, grey) was used as nuclear counterstain. The* IMPDH1 *signal was present in the photoreceptor inner segments, outer plexiform layer and processes reaching into the outer nuclear layer (ONL), as well as in the ganglion cell layer (GCL) and inner nuclear layer (INL) (**a, b, c**). The higher magnification pictures (x63) suggest that* IMPDH1 *was present in clotted mesoscale filaments (**d, e, h, i**).* IMPDH1 *expression is less detailed in rd1 in vivo cross sections (**f**). At P18 the ONL degraded to a single cell layer with no discernible expression pattern being present in the ONL and segments (**g**). Retinal pigment epithelium (RPE), postnatal day (P).*

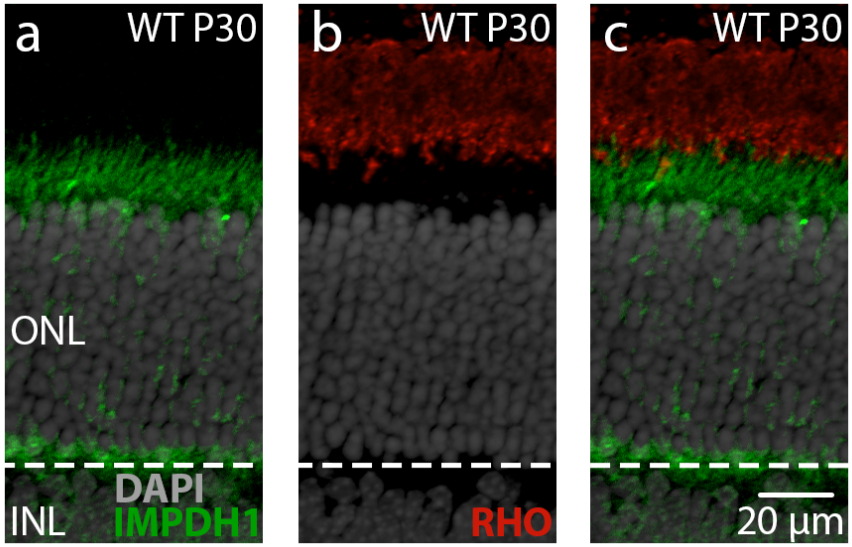

Figure 10: Colocalization of inosine monophosphate dehydrogenase 1 and rhodopsin

*Inosine monophosphate dehydrogenase 1 (*IMPDH1*, green) in wild-type (WT) in vivo retinal cross-sections was expressed in the inner segments of photoreceptors but not in the outer segments (**a**). 4',6-diamidino-2-phenylindole (DAPI, grey) was used as nuclear counterstain. The rhodopsin (*RHO*, red) signal reached into the transition region between inner and outer segment layers (**b**). The signals only overlap in offshoots between inner and outer segment, localizing to the*

*region of the connecting cilium (**c**). Outer nuclear layer (ONL), inner nuclear layer (INL) postnatal day (P).*

3.1.1 IMPDH1 proximity with Müller glia cells

After staining for IMPDH1 and examining the signals reaching into the ONL from the segment layer, it was hypothesized that the enzyme could be connected to Müller glia cells. To investigate this possibility, a colocalization with the Müller cell marker glutamine synthetase was performed. In the brain, GS is mainly expressed in astrocyte glia cells, and in the retina, it is known to stain the Müller glia cells (Germer et al., 1997). While the signal was mainly present in the same layers, namely reaching from the GCL, through INL, OPL and in between the DAPI stained cell cores to the transition zone of the ONL to the segment, it was less of an exact colocalization and seemed to be barely adjacent. These results can also be deduced from the occurrence of the corresponding genes, which are missing in the Müller glia cells according to (proteinatlas.org, Karlsson et al., 2021). The two enzymes nonetheless were in close proximity to each other in the various retinal layers.

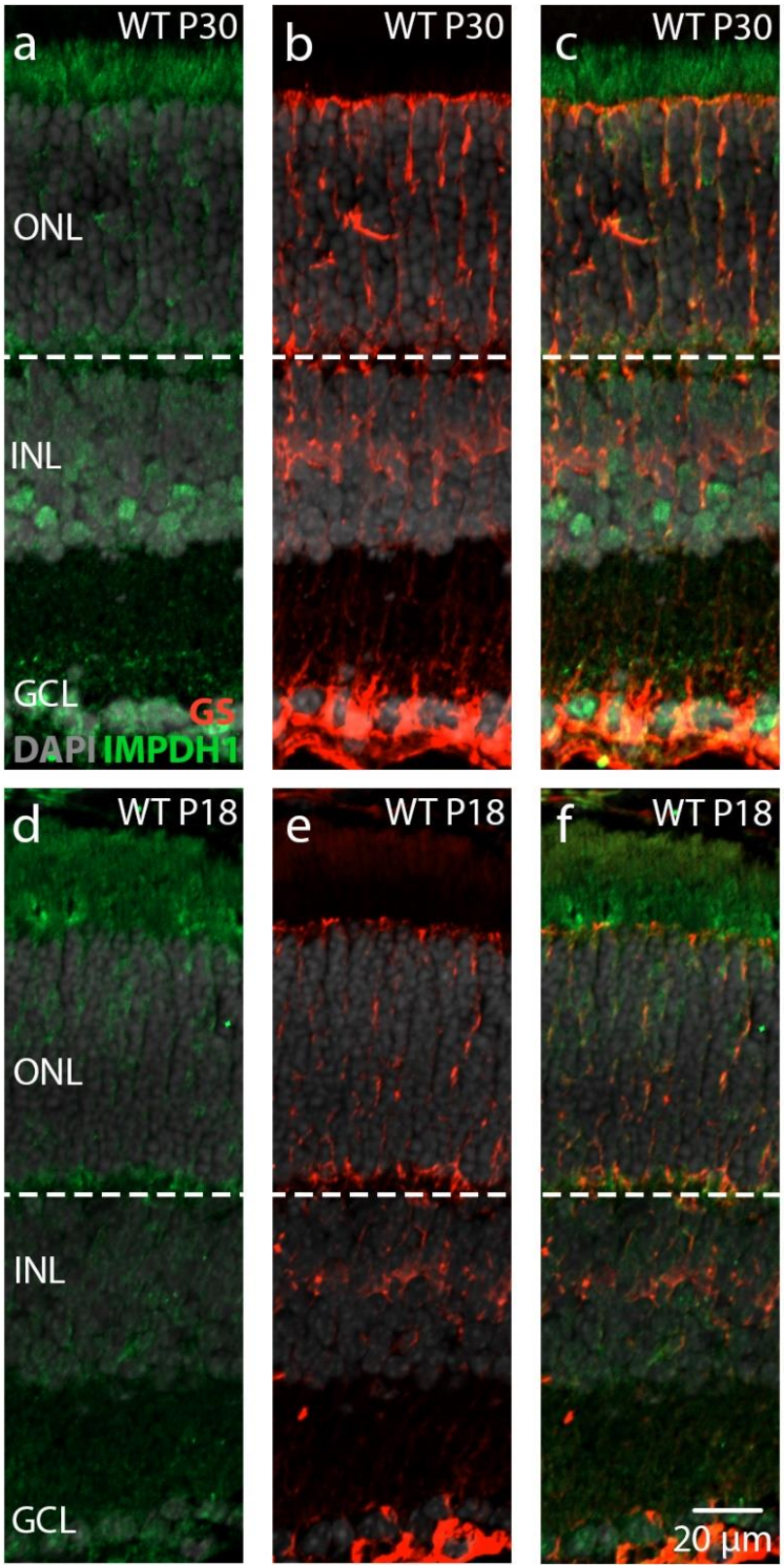

Figure 11: Colocalization of inosine monophosphate dehydrogenase 1 and glutamine synthetase

*In wild-type (WT) retina, in vivo, at ages from P18 to P30, inosine monophosphate dehydrogenase 1 (*IMPDH1*, green) signal was present throughout the retina, with a more marked expression in photoreceptor inner segments (**a, d**). Glutamine synthetase (*GS, red*) labeled the Müller glia cells of the retina, reaching through the entire retina from the ganglion cell layer (GCL) up to the outer nuclear layer (ONL) mice (**b**, **e**).* IMPDH1 *showed signals close but not overlapping with the* GS *offshoots in the ONL (**c, f**). Inner nuclear layer (INL), postnatal day (P). 4',6-diamidino-2-phenylindole (DAPI, grey) was used as nuclear counterstain.*

3.2 GC is expressed in outer segments

Further down the cGMP synthesis pathway, the last step from GMP to cGMP, is catalyzed by GC. This enzyme is ubiquitously expressed in most of the human body, including in the retina. Retinal membrane guanylyl cyclase (RetGC), which is expressed in photoreceptor cell membranes and facilitates the cGMP production, is a version of this enzyme specific for the retina and only expressed in photoreceptors.

I stained a subunit of RetGC called particulate guanylyl cyclase E (PGCE), which is only present in rodents to prove that the full cGMP catalyzing pathway can take place in the photoreceptors. PGCE was expressed in the segments of P11 WT mice. At this age, the signal in *rd1* animals was of similar structure as in the WT but with irregularly occurring signal interruptions. This could be seen in high magnification microscopic images and emphasized the regularly lined up segments of the WT, compared to the *rd1* mutant. This result was reproducible in multiple stainings. To further differentiate the segment localization, a colocalization with rhodopsin was performed. Both signals overlapped in the outer segment region. PGCE expression was observed in short parallel strokes, directly situated on the ONL in a grass like formation similarly to how IMPDH1 stained the inner segments. Small offshoots reaching into the inner segment layer were indicative of the connecting cilium structure between the segments. Rhodopsin, although clearly colocalized, showed a rather flat structure with extensions that pointed in the direction of the RPE. The elongated vertical structure of the photoreceptor

outer segments stained by PGCE lengthened with age and appeared more differentiated at P30.

IMPDH1 and GC were topographically close to each other through their expression in the inner and outer photoreceptor segments respectively. Since both enzymes are instrumental in catalyzing cGMP production, they may form a functional unit.

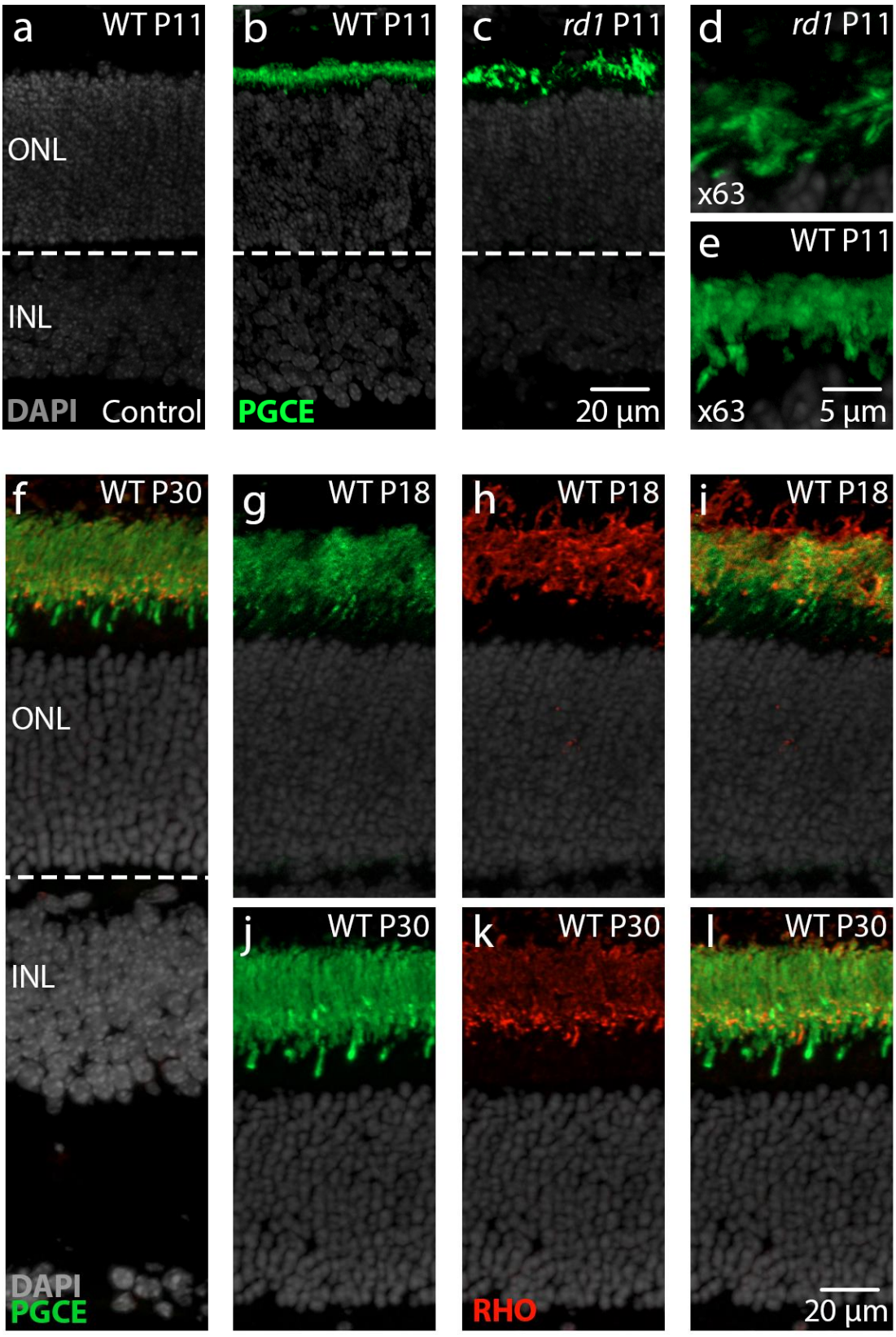

Figure 12: Particulate guanylyl cyclase E and colocalization with rhodopsin

*Particulate guanylyl cyclase E (*PGCE*, green) was expressed in the outer segments of photoreceptors in wild type (WT) mouse retina. At P11,* PGCE *signals localized to inner segments which are not yet fully developed at this age (**a, b**). The signal in the rd1 model appeared uneven compared to WT (**c, d, e**). In P18 and P30 mice the* PGCE *signal colocalized with rhodopsin (*RHO, red*) except for offshoots reaching into the inner segments (**f - l**). Outer nuclear layer (ONL), inner nuclear layer (INL), Postnatal day (P). 4',6-diamidino-2-phenylindole (DAPI, grey) was used as nuclear counterstain.*

3.3 TUNEL *in vivo* baseline

Before starting *ex vivo* retinal explant cultures and their treatment, the goal was to establish a baseline of cell death occurring *in vivo* in the retina of *rd1* animals. The TUNEL assay reliably stains dying cells in this model, where cell death is known to peak at around P13 (Arango-Gonzalez et al., 2014).

There is a significant difference in the percentage of TUNEL positively stained cells between the wild type and the *rd1* model as seen on the right in Figure 13. In WT mice at this age the retina is still in development and some cells divide while others undergo developmental apoptosis, which can be seen in a low amount of TUNEL stained cells. In the later experiments performed using retinal explant cultures, this phenomenon will add to the baseline of dying cells as well as those, that are caused by the artificial nature of the culturing process and environment. The TUNEL data also demonstrates that in the *rd1* model at P11 5.69% (± 0.11 SD) of the photoreceptor cells in the ONL cells are already in the process of dying in a cGMP related manner, considering the causative mutation. This percentage is close to the expected cell death peak at around P13 which may be caused by variations in the age of the animals or a low sample number bias. Although this amount cannot be directly compared with the explant cultures, it indicates the range of results and difference between WT and mutant which can be expected. Individual values and the descriptive statistics of these quantifications can be found in Table 6 in the annex.

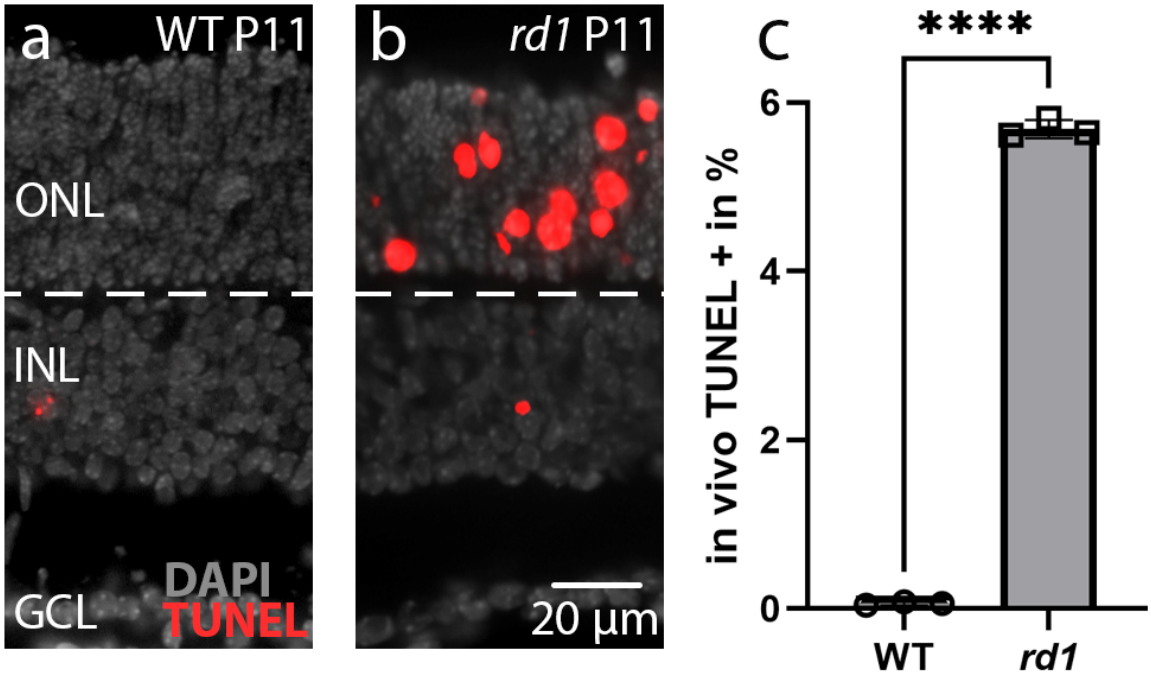

Figure 13: Cell death comparison in vivo

*In vivo cross-sections showing TdT-mediated dUTP-biotin nick end labeling (TUNEL, red) stained cells, the wild type (WT) showing no TUNEL stained cells in the outer nuclear layer (ONL) and the rd1 model a high number of cells the ONL in the process of dying in these single layer microscopy images (**a, b**). Unpaired two-tailed students t-test with significant difference of TUNEL positive cells in the ONL of P11 WT and rd1 in % **(c)**. Inner nuclear layer (INL), ganglion cell layer (GCL), 4',6-diamidino-2-phenylindole (DAPI, grey) was used as nuclear counterstain. **** p<0.0001.*

3.4 Mycophenolic acid treatment

To assess treatment efficacy, different concentrations of MPA were added to the medium during the medium exchanges. The *rd1* retina explants were treated with 1 µM, 10 µM, 40 µM, 78 µM, 250 µM, and 1000 µM of MPA in the CM. Additionally to these treated explants, controls with just CM or CM and the solvent DMSO were cultivated as well. The highest dose was used to assess a possible toxic effect of the treatment. We expected that a close to tenfold increase in the

effective dose could result in toxic effects in the form of detectable cell death. This was deemed necessary for the completion of the full dose response curve. The explant treatments were repeated between n = 6 and n = 9 times. This discrepancy stems from some explant cultures not being usable. The explants with lower doses of MPA had a similar retinal structure compared to the untreated controls. However, the highest dose of 1000 µM presented a clear collapse of the usual retinal structure. The layers conflated into each other and smaller structures like the inner plexiform layer were not recognizable anymore. Only the ganglion cells were still distinguishable from the other layers and structures. Aside from structural abnormalities, the amount of TUNEL positively stained cells was extremely elevated.

In wild-type sections, TUNEL positive cells were expected for two reasons: An artificial *ex vivo* situation with unpreventable damages during preparation or cultivation, as well as the ongoing retinal development process at this age. The amount of dying cells seemed to decrease in a dose-dependent manner while the 40 µM, 78 µM, and 250 µM MPA concentrations visually resembled the wild-type situation.

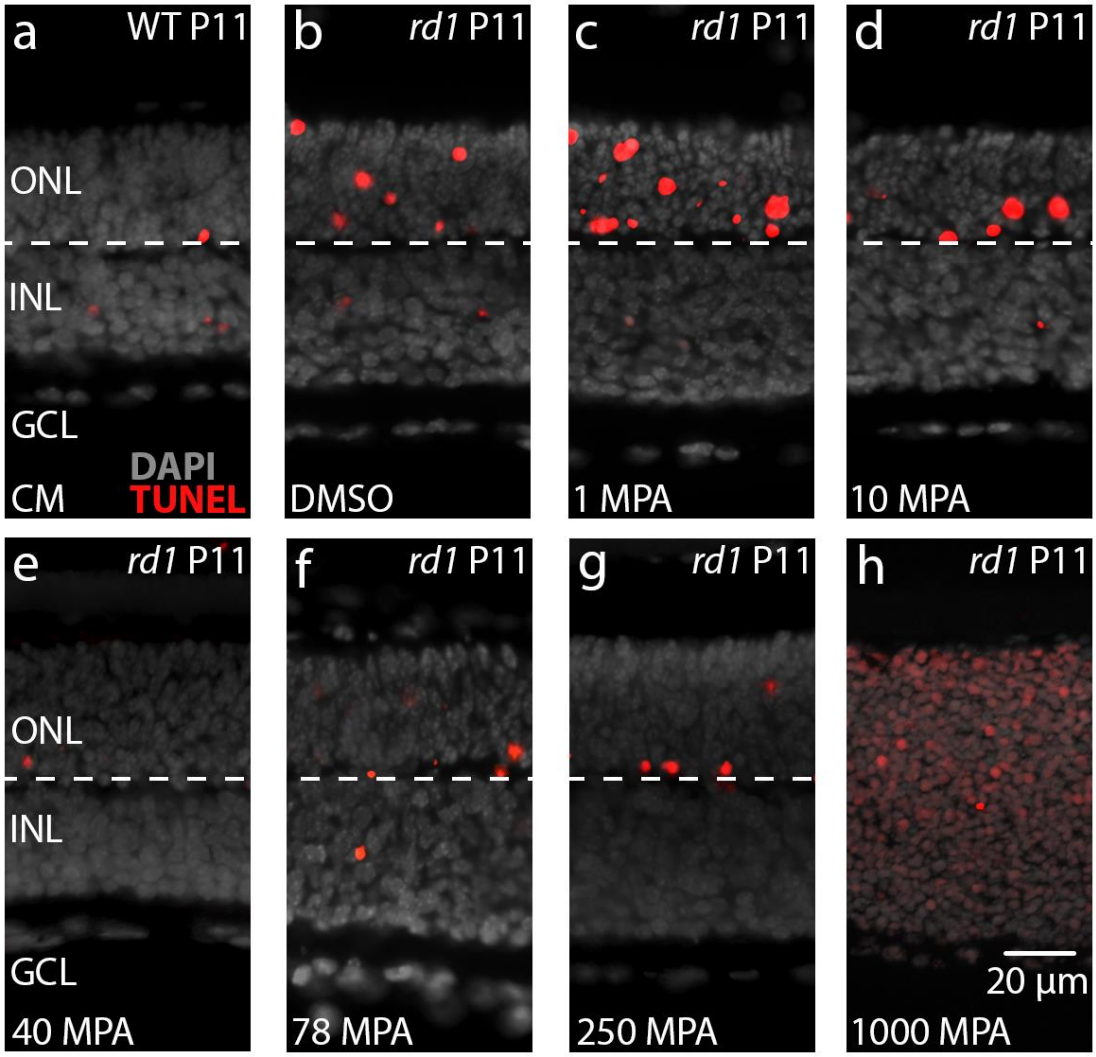

Figure 14: Overview for explant culture TUNEL staining

Pictures showing postnatal day (P)11 retinal explant cultures stained with TdT-mediated dUTP-biotin nick end labeling (TUNEL, red). Wild-type (WT) retina was cultured in complete medium (CM) and displayed only a low number of dying, TUNEL positive cells in the outer nuclear layer (ONL) ***(a)****. Rd1 mouse retina exposed to either dimethyl sulfoxide (DMSO) or different concentrations of Mycophenolic acid (MPA) showed extensive cell death. The number of dying cells was reduced at MPA concentrations of 40 µm or higher* ***(b - g)****. Yet, at 1000 µm MPA there was a marked loss of retinal structure with no distinguishable layers remaining except for the ganglion cell layer (GCL)* ***(h)****. Inner nuclear layer (INL), 4',6-diamidino-2-phenylindole (DAPI, grey) was used as nuclear counterstain. The WT explant sections used for staining were provided by Lan Wang.*

3.4.1 Medium and solvent controls

Control samples cultivated with either CM or CM and DMSO were used for comparison with MPA treated retinas. Since no significant difference emerged between those two controls, neither in the TUNEL positive cell count nor in the ONL photoreceptor row count (Figure 15**a** and **b**, respectively), these samples were combined into a single “control” group. This allowed for the sample size of the control group to reach n = 17. Individual values and the descriptive statistics of these quantifications can be found in Table 7 in the annex.

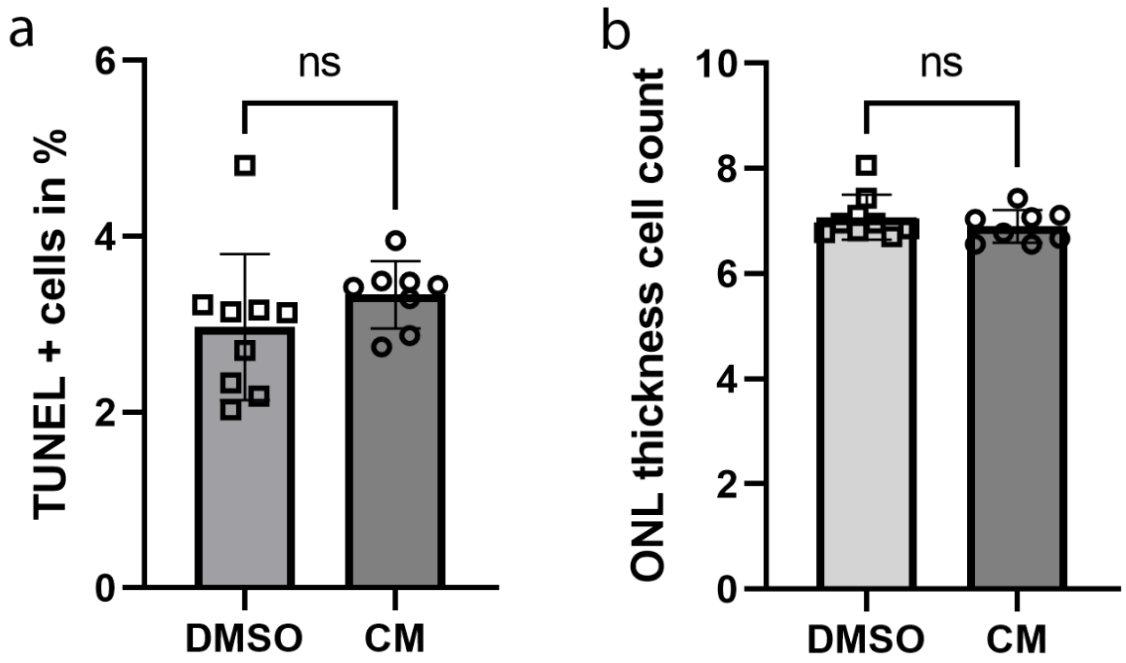

Figure 15: Control comparison for TUNEL stained cells and ONL thickness

Both dimethyl sulfoxide (DMSO) and complete medium (CM) treated retinal cultures were used as controls. Student’s t-test performed between the two groups for both TdT-mediated dUTP- nick end labeling (TUNEL) positive cells and outer nuclear layer (ONL) thickness indicated no significant (ns) differences between DMSO treated and CM retinal explants.

3.4.2 MPA reduces cell death in *rd1*

For the comparison of the different MPA concentrations against the control, all TUNEL positive stained cells in the ONL were counted and their percentage calculated. As a comparator, the cell death percentage of WT retina explants was added. The merged control group presented an average cell death of 3.14% (± 0.67 SD). The lowest dose of 1 µM MPA showed a higher average cell death of about 3.5%, but without a significant difference in statistical analysis. The cell death average of 10 µM MPA was lower than the control with 2.40% (± 0.99 SD) but did not show any significant difference. TUNEL positive cell death was significantly reduced when treated with concentrations between 40 µM and 250 µM of MPA (Figure 16**a**). The *p*-value of the 40 µM MPA dose was calculated to be less significant than 78 µM and 250 µM MPA doses, which was most likely caused by a lower sample number of n=6. The effective doses lead to very close average cell death percentages of 1.47% (± 0.53 SD) for 40 µM, 1.46% (± 0.43 SD) for 78 µM and 1.45% (± 0.27 SD) for 250 µM MPA, indicative of a plateau effect in rescuing photoreceptors. Cell death in wild type averaged at approximately 0.85%. Nevertheless, a cell death reduction to an amount considered in the range of a healthy retina could not be reached. The dose-response curve in Figure 16**b** may illustrate this situation.

Only the highest dose of 1000 µM lead to massive general cell death in all layers of the organotypic retinal explant culture. This dose did not achieve a significant difference presumably due to the spread-out distribution of residuals as seen in the residual plot and quantile-quantile (QQ) plot in Figure 19 in the annex. These results visually suggested MPA toxicity at high doses, even though this effect was not statistically significant. Individual values and the descriptive statistics of these quantifications can be found in Table 8 in the annex.

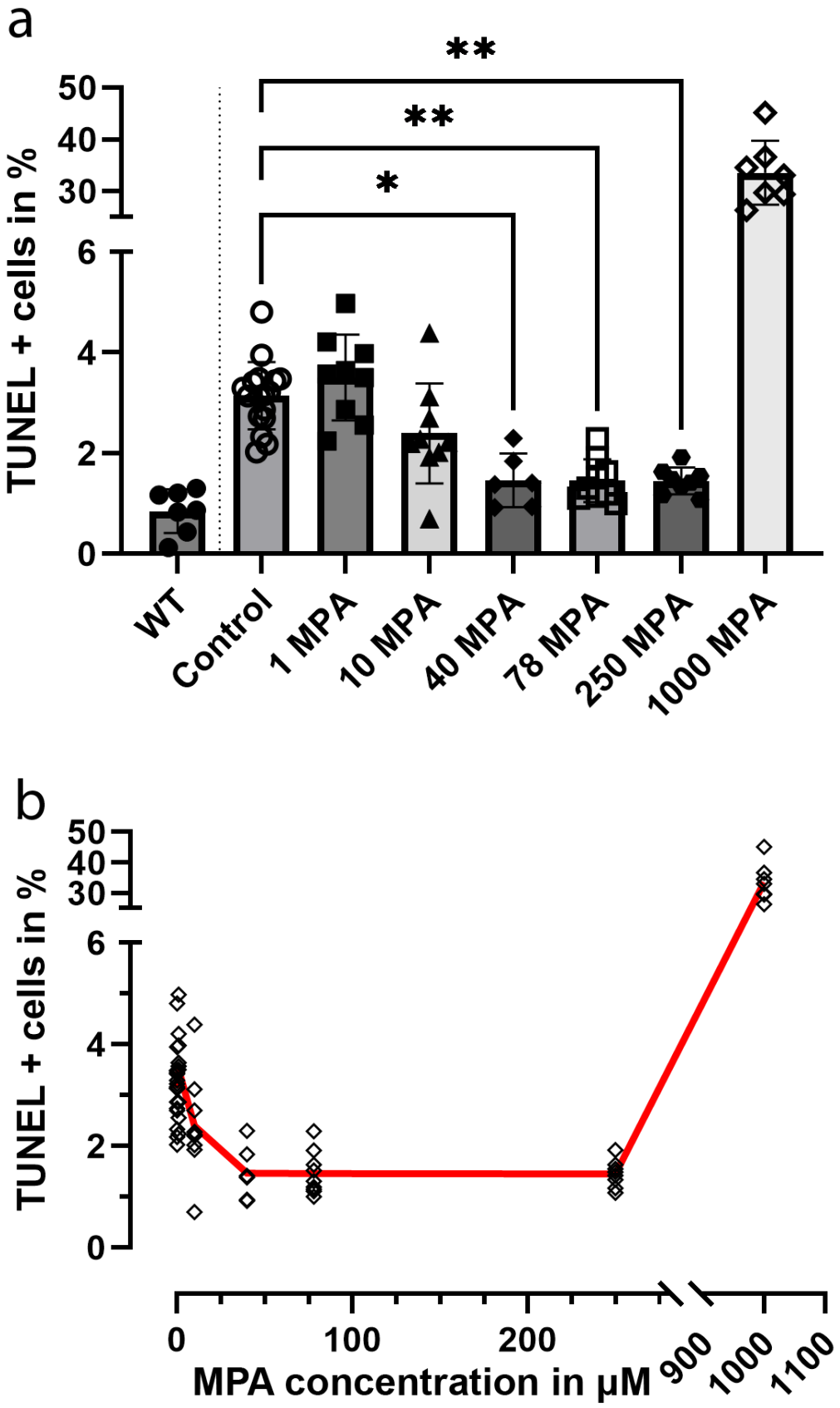

Figure 16: TUNEL positive cell % comparison and dose-response curve

*Percentage of TdT-mediated dUTP-biotin nick end labeling (TUNEL) positive cells in the ONL. Mycophenolic acid (MPA) treatment on rd1 mouse retina at different concentrations compared to an untreated control **(a)**. An ANOVA Kruskal-Wallis test with Dunn`s multiple comparisons test against the control group was performed and showed significant differences for MPA concentrations 40 µM, 78 µM, and 250 µM. A dose-response curve using the same TUNEL data as in **(a)** illustrating a plateau effect between 40 to 250 µM MPA **(b)**. Wild type (WT) data **(a)** shown for comparison only. The WT explant sections used for quantification were provided by Lan Wang. * $p < 0.05$; ** $p < 0.01$.*

3.4.3 MPA maintains photoreceptor rows

To consider the possibility that a part of the cell death processes had already taken place and resulted in the loss of ONL cells (and could hence not be detected by the TUNEL staining anymore), the photoreceptor rows of the ONL were quantified and compared. The number of cells aligned vertically in the ONL of the retina and stained by DAPI were counted.

The control group average value was 6.99(± 0.38 SD) rows in the ONL. The doses 1 µM and 10 µM MPA presented a similar ONL row count as the control group with no significant difference between them. As it was the case in the TUNEL-stained cell comparison, 40 µM, 78 µM, and 250 µM MPA doses resulted in a thicker ONL with a significant difference compared to the control group (Figure 17**a**). The dose response curve (Figure 17**b**) for these groups displayed a plateau, in line with the cell death results, averaging at 8.77 (± 0.49 SD) for 40 µM, 8.90 (± 0.77 SD) for 78 µM and 8.95 (± 0.42 SD) for 250 µM rows in the ONL. In the case of the 1000 µM MPA dose, ONL thickness was counted by estimating the ONL border to the OPL as the degraded retina's structure did not allow reliable differentiation between the merged layers. It was tested against the untreated control group and showed a significantly reduced photoreceptor row count, suggesting toxicity of high MPA concentrations.

In prolonged treatment exposure this effect would likely be exacerbated. The large numbers of TUNEL positive cells observed at P11 are in the process of dying and presumably would have disappeared 1-2 days later. All values of the ONL photoreceptor row count lay close to each other in their respective groups, leading to higher significance in the performed tests. Individual values and the descriptive statistics of these quantifications can be found in Table 9 in the annex.

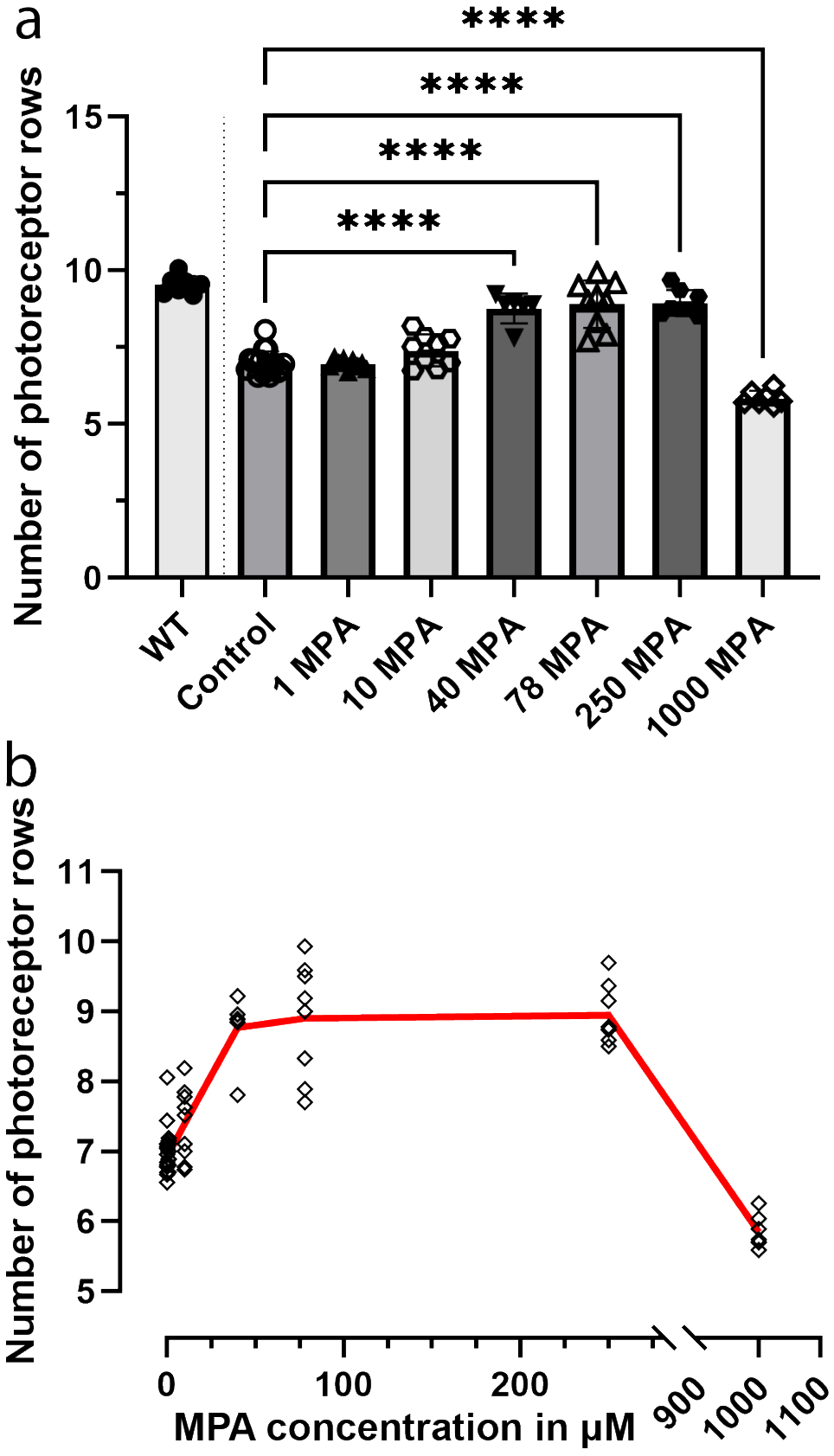

Figure 17: ONL thickness cell count comparison and curve

*Photoreceptor row counts in the outer nuclear layer (ONL) for different Mycophenolic acid (MPA) concentrations used to treat rd1 ex vivo cultured retina explants, compared to untreated control (**a**). An ordinary one-way ANOVA with Brown-Forsythe and Bartlett's test with Dunnett's multiple comparisons test against the control group was performed and showed significant differences for MPA concentrations 40 µM,78 µM**,** 250 µM, **a**nd 1000 µM. A dose-response curve using the same ONL thickness cell count data as in **(a)** presented a plateau effect between 40 to 250 µM MPA with only slight increase for drug concentrations above 40 µM MPA (**b**). Wild type data (WT) in **(a)** shown for comparison only. The WT explant sections used for quantification were provided by Lan Wang. **** p < 0.001.*

3.4.4 Cones are unaffected by MPA treatment

To evaluate the effect of the MPA treatment on cone photoreceptor cells, a quantitative assessment by counting the cone cells was necessary. First, a cone arrestin (ARR3) staining was performed. The antibody detects the protein arrestin-C, which is expressed in the cell bodies on cone photoreceptors. On some of the explant sections this resulted in different signal structures, with low intensity making the cells barely visible. This weak arrestin-3 labelling was likely due to the fact that in the P11 retina used here cones are not yet fully differentiated and hence only express low amounts of arrestin. This led me to try a different cone-staining with higher intensity and better consistency between the different explant sections for reliable quantification.

Peanut agglutinin (PNA) labels lectins expressed in the inner and outer segments of cone photoreceptor cells, as well as in the synaptic regions, leading to signals in the OPL and the region between INL and GCL (Blanks and Johnson, 1984). The peanut agglutinin was directly conjugated with fluorescein, such that the PNA staining could be performed in a single step. Retinal structure and cone segment signals looked similar in the different situations as seen in Figure 18. Compared to the non-cultured *in vivo* situation, the *ex vivo* cones segments appeared flattened or shorter (data not shown). The number of cones was

counted per 100 µm to compare between wild type, *rd1* with DMSO control, and the lowest effective cell death reducing dose of MPA (40 µM). In these three experimental groups, cone counts were 6.85 (± 1.23 SD) for WT, 7.32 (± 1.39 SD) for DMSO control and 6.65 (± 0.61 SD) for 40 µM MPA cones per 100 µm. The groups were tested against each other with no significant differences.

It is assumed that cones only die off as a consequence of the structural changes that occur in the course of the disease subsequent to the disappearance of rods, given that the *Pde6b* mutation in *rd1* mice is only present in rod photoreceptors. Thus, if the explant culture was extended for a longer period of time, a reduced amount of cone cells should be observable. These results showed that the four-day long treatment with MPA did not significantly affect the survivability of cone photoreceptors. Individual values and the descriptive statistics of these quantifications can be found in Table 10 in the annex.

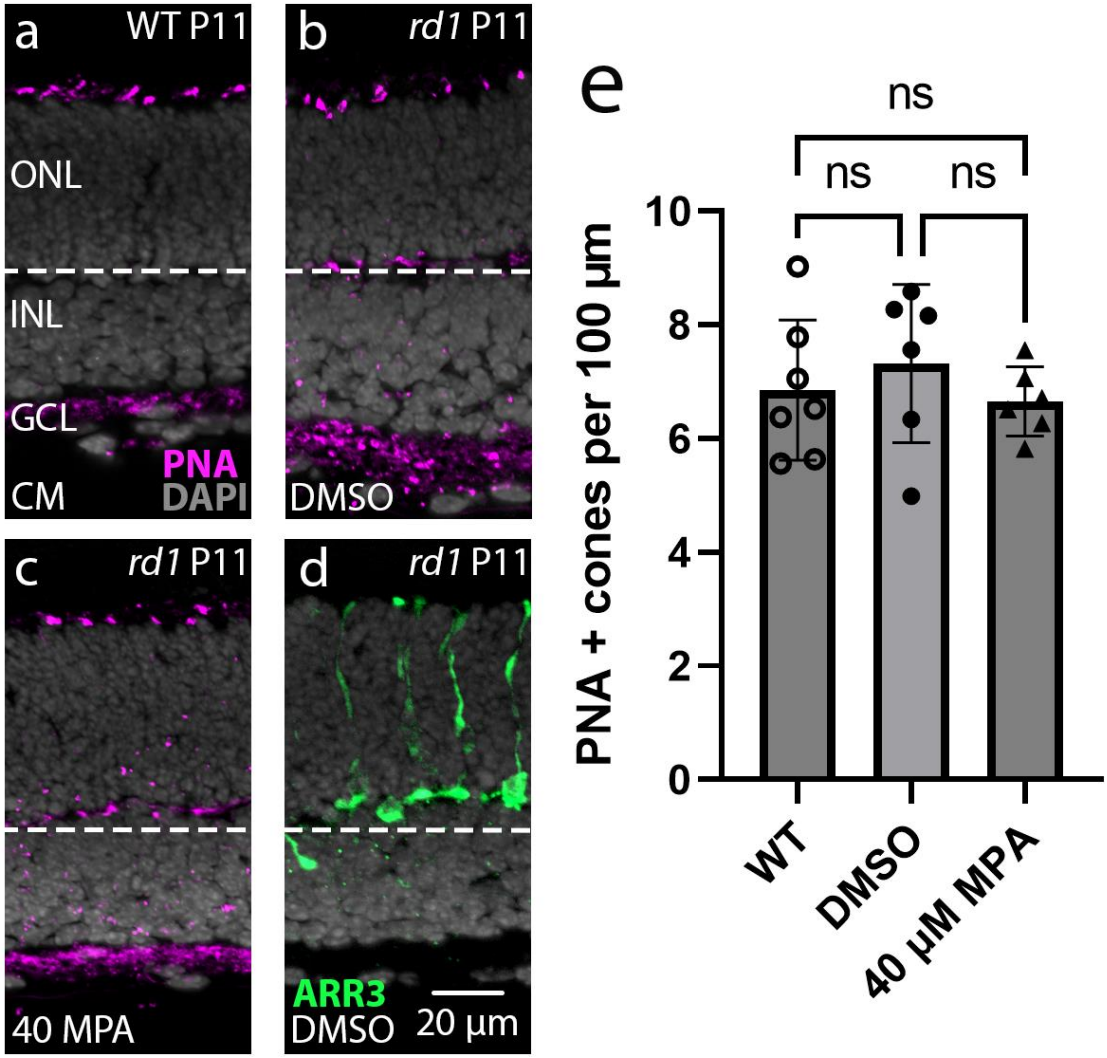

Figure 18: Cone staining and quantitative analysis of the cone count

*Peanut agglutinin (*PNA*) labeled the outer segments of cone photoreceptors in ex vivo cultured retinal explants. Also labelled were the outer plexiform layer (OPL) and the region of the inner plexiform layer (IPL) (**a, b, c**). Cone arrestin (*ARR3*) also stains cone photoreceptors, but here the staining could be seen more strongly in the cell body and synapses **(d)**. 4',6-diamidino-2-phenylindole (DAPI, grey) was used as nuclear counterstain. The quantification of PNA stained explant cultures indicated around 5-8 cones per 100 µm in wild type (WT), dimethyl sulfoxide (DMSO, solvent) control, and 40 µM Mycophenolic acid (MPA) **(e)**. An ordinary one-way ANOVA with Brown-Forsythe and Barlett's with Tukey's multiple comparisons test between each data set was performed resulting in no significant difference between the groups. Complete medium (CM), inner nuclear*

layer (INL), ganglion cell layer (GCL), Postnatal day (P). The WT explant sections used for staining were provided by Lan Wang.

3.4.5 Treated medium and control pH

For the successful cultivation of explants, a constant pH level is necessary. This is provided by the buffering capacity of the culture medium. This accounts for any changes occurring naturally. To rule out that high MPA amounts had any effect on the pH, it was tested for all mediums using a pH meter. There was no measurable difference in the pH between the different doses, the DMSO control and the untreated CM control (Table 5).

Table 5: pH level vs. concentrations of MPA and solvent

For each medium exchange approximately 1.2 ml of complete medium (CM) with the corresponding added substances was prepared. Total volume of Dimethyl sulfoxide (DMSO) added to the medium used for treatment and their proportionate quantity in percent as well as measured pH level of the treated media are shown. Mycophenolic acid (MPA).

1,2 ml CM	**CM**	**DMSO**	**1 µM MPA**	**10 µM MPA**	**40 µM MPA**	**78 µM MPA**	**250 µM MPA**	**1000 µM MPA**
Vol. added	-	4.4µl (DMSO)	0.24µl (5µM MPA)	2.4µl (5µM MPA)	9.6µl (5µM MPA)	4.41µl (21µM MPA)	14.28µl (21µM MPA)	57.14µl (21µM MPA)
pH	8.2	8.2	8.2	8.2	8.2	8.2	8.2	8.2
DMSO in %	0	0.37	0.02	0.2	0.8	0.37	1.19	4.76

Table 5 above also shows the different concentrations of the solvent DMSO used for the different doses. DMSO is widely considered a safe solvent in concentrations up to 1%, with higher concentrations decreasing the proliferation of cultured cells. As the focus of the experiments was not on proliferation but cell death, this trade-off was accepted. In the case of the 1000 µM MPA dose, DMSO concentrations reached close to 5%. Although higher concentrations are accepted in live animal experiments, they can show a dose dependent toxicity including cell death in cell culture (Da Violante et al., 2002, Qi et al., 2008). Since this cannot be ruled out, the amount of cell death seen with the highest MPA dose could also be due to DMSO toxicity.

4 Discussion

In this study, I confirmed the location of IMPDH1 and GC in the photoreceptor segments and their suitability as a target for drug treatments. I tested different concentrations of MPA in organotypic retinal explant cultures of *rd1* mice and found a significant neuroprotective effect at MPA concentrations ranging from 40 µM and 250 µM. I was able to show significantly reduced photoreceptor cell death and a preservation of ONL photoreceptor rows in this concentration range. The lowest effective dose of 40 µM MPA had no cell death inducing effect on cone photoreceptors. This drug concentration could serve as a starting point for further research, with the objective of achieving the strongest protective effect with the least amount of adverse effects.

4.1 Cell death mechanisms in *rd1*

The pathology of RP is characterized by an initial rod death with cone death following once all or most rods have been lost. As the genetic causes are diverse and the pathological mechanisms are not fully understood, different theories on why rod cell death occurs have been publicized and connected to RP. These include apoptosis (Choudhury et al., 2013), necrosis (Murakami et al., 2015), regulated necrosis (*e.g.* necroptosis) (Viringipurampeer et al., 2019), ferroptosis (Obolensky et al., 2011), PARthanatos (Jiao et al., 2016), and cGMP-dependent cell death as potential causative degeneration pathways. The initiation of PARthanatos may overlap and depend on pathways also occurring in cGMP-dependent cell death via CNG channel activity (Figure 4) (Yan et al., 2022). An important aspect of investigating these mechanisms is the identification of early, upstream events that initiate the degenerative cascade due to their potential for future treatment (Newton and Megaw, 2020).

TUNEL staining labels apoptotic and non-apoptotic cell death mechanisms in cells if DNA nick-ends emerge during the process of dying (Gavrieli et al., 1992, Grasl-Kraupp et al., 1995). In my experiments, I inhibited IMPDH1 activity with

MPA, which led to a reduced number of dying cells in *rd1* mouse retina as seen in Figure 16**a** and (Yang et al., 2020). This in turn suggests an influence of cGMP on cell death and thus possibly a cause of cell death in photoreceptors with the corresponding cGMP elevating and dysregulating mutations. This data reinforces the previously established cGMP-dependent cell death (Tolone et al., 2019). Another point to note is the plateau effect of MPA in effective doses, which suggests that the reduction in IMPDH1 activity is limited (Figure 16**b**, Figure 17**b**). Drastically reduced cGMP concentrations lower than physiologically normal through *e.g.* GC mutations may also activate cell death pathways (Agrawal et al., 2017). The potentially limited IMPDH1 inhibition of MPA may therefore reduce the risk of local adverse side effects through low cGMP concentrations. These pathways and the effect of MPA may be transferrable to other retinal degeneration models, and, if applicable, to human RP, where MPA treatment could provide for a broad, mutation-independent progression-delaying treatment option.

4.2 Role of IMPDH1 in Retinitis pigmentosa

The enzyme IMPDH1 plays a key role in the retina through rate-limiting the synthesis of guanosine derived molecules. This is especially important for the visual transduction process as it is based on the modulation of intracellular cGMP-levels. While the gene *IMPDH1* is expressed not only in the retina, all of its known mutations lead to IRDs like RP or LCA (Sakti et al., 2023). Why the retina is more susceptible to such mutations compared to other tissues is unknown. One possibility for this may be the high energy throughput required to maintain the functionality of the retina. This suggests a higher susceptibility of retina and photoreceptors to changes in the absolute amount of cGMP. However, an *IMPDH1*$^{-/-}$ mouse model shows a slower progressing course of the disease, suggesting that the more severe defect in human *RP10* may be caused by a gain of function after protein misfolding and subsequent aggregation (Aherne et al., 2004). The inhibitory effect on IMPDH1 by MPA might be able to normalize the activity of the mutated enzyme, provided that the mutant protein is still capable of binding MPA. The close proximity of IMPDH1 to GC in the photoreceptor segments suggests

that they might form a functional unit providing important steps for the synthesis of cGMP. Other enzymes necessary for cGMP metabolism like GMP synthase may also be part of this unit (Plana-Bonamaiso et al., 2020).

4.3 Mycophenolic acid as a treatment for RP

MPA might offer neuroprotective effects in forms of RP related to cGMP-dependent cell death and may be able to slow down disease progression. In this study, the findings of (Yang et al., 2020), namely reduced cell death and reduced cGMP levels in *rd1* animals could be confirmed. In addition, Yang and colleagues found a rescue of scotopic vision in electroretinogram investigations. In my own investigations I was able to narrow down the effective MPA dose to 40 µM up to 250 µM, as this is where the dose plateau in *ex vivo* cell death reduction occurs. This therapeutic range appears sufficiently large to accommodate for some changes in bioavailability and biokinetics of the substance when translated to humans. With 40 µM, a new minimum concentration needed to reach a maximal reduction in cell death and maintaining ONL photoreceptor rows was established. Even with a severe and rapidly progressing mutation, as in the *rd1* retina, a significant protection could be demonstrated. Yet, cell death levels could not be reduced as far down as is common in wild type retina and therefore the treatment must be considered as *delaying* but not *stopping* photoreceptor cell death. Another factor is that the treatment was started at P7, with rod degeneration starting at around P6, this is early in the progression of the disease and such a timing requires early and correct diagnosis to delay the retinal degeneration as much as possible. With a slower progressing, disease model such as the *rd10* mouse, it may be possible to further improve the treatment´s effectiveness (Yang et al., 2020). As the pathway leading to cell death in PDE6A mutations is also based on high cGMP levels, the results with these models should be similar here as well.

The high dose toxicity of MPA has previously been shown in other animal species and its side effect profile is well established in humans as it is an already approved medication. Nonetheless, since the concentration of the solvent DMSO in our experiments was close to 5%, a contribution from solvent toxicity cannot be

ruled out entirely. The potential dose-dependent toxicity of DMSO is somewhat controversial, in some cases cell death was provoked by concentrations of 6% (Qi et al., 2008), while in other cases no significant alteration of the cells could be shown at concentrations of 10% in the culture medium (Da Violante et al., 2002). The actual toxicity might also depend on the proliferation rate of the cultured cell (de Abreu Costa et al., 2017). The retina of humans would already be fully developed on birth, which is not the case in rodents, and hence the animal´s age may be a decisive factor for MPA drug toxicity. The mice used in our experiments are of the C3H mouse line, in which the retina is considered to be fully developed at age P30, a significant amount of cell proliferation still takes place during the first 2-3 weeks post-natal (Cepko et al., 1996).

Even though retinal gene therapy with Luxturna for *RPE65*-dependent LCA had its first success and has shown great potential for further gene replacement therapy, the visual acuity rescue is limited. Moreover, Luxturna use is associated with a significant risk for serious adverse effects such as chorioretinal atrophy (Dormegny et al., 2024). Thus, there is a need for (complementary) neuroprotective medications that can be applied to multiple distinct RP forms and that could supplement gene therapies.

4.4 Outlook

While the various positive results obtained for MPA in *in vivo* and *ex vivo* experiments are very promising, for human clinical use, there are many more steps to be taken into consideration to be able to ensure efficacy and safety. Several options are available to apply the substance in humans, which range from oral or intravenous systemic treatment to further localized options like topical or intravitreally injected treatment.

Systemic treatment is an option but is associated with important side effects as seen in organ transplant patients (Panackel et al., 2022), as well as potentially lacking in potency at the target location, the photoreceptors of the retina. Only minor amounts of MPA may reach the eye even without consideration of the BRB,

which is permeable for MPA though. To achieve the desired neuroprotective effect, MPA must reach the rod photoreceptors in effective concentration. Thus, further ocular pharmacokinetic studies are required to assess the actual amount of drug reaching the photoreceptors.

Given the various ocular barriers, topically applied MPA is unlikely to reach the retina (Himawan et al., 2019), while provoking local side effects, as lacrimal fluids flow rate would deliver the active ingredient to the nasal mucosa via the tear duct (Agrahari et al., 2016). This leads to reduced efficacy at the eye and can even induce systemic adverse effects after mucosal absorption.

Other possibilities for drug administration include: The subconjunctival route (Raghava et al., 2004), retrobulbar route (Okada et al., 2003), peribulbar and sub-Tenon routes (Johnson and Chu, 2010), and intracameral route (Chang et al., 2009).

The most common and best investigated application route is the intravitreal injection mostly used for anti-VEGF treatments. In case of exudative age related macular degeneration this is done with a loading phase of at least 2 injections in monthly intervals (Hao and Bailey, 2023). This is followed by monitoring to evaluate efficacy and necessary follow-up treatments, which, in most cases, can be done with longer periods in between drug injections.

Repeated injections can lead to intraocular infections, cataract, retinal detachment and hyperemia (Maurice, 2001). This makes conjugating MPA to a drug delivery system, that offers a sustained release and distribution effect, necessary for long term use in RP patients. A custom-tailored drug delivery system based on targeted lipids may also allow for systemic treatment with focused uptake in the RPE and retina, this could still provoke some adverse systemic effects, but would circumvent the risks of repetitive injections into the eyeball (Bohley et al., 2022). Investigating the delivery to photoreceptor cells and the effect of such an administration route could be a target for further research.

While the murine metabolic rate is approximately 7-times higher compared to human (Demetrius, 2005), how this affects tissue after permeating the BRB is unclear. In general, it is safe to assume that any dose would stay effective over a

longer period in humans compared to mice. The collected data for concentration efficacy though is transferrable from mice to human as effects on a cell-based level are likely to be similar. Yang's publication showed what concentration per body weight needed to be injected into the animal to achieve an effect, but the actual retinal dose was unclear. With my new data, it is possible to approach what concentrations are required to achieve a therapeutic effect in the retina. Here, the plateau effect of MPA may allow for a broader therapeutic window. It is of note, that in the case of explant cultivation, the retina is surrounded by medium and is mostly supplied from the choroidal side of the retina, while in an intravitreal injection, the drug would reach the retina from the vitreous.

The average human vitreous chamber volume (VCV) is 4.65 ml in females and 4.97 ml in males (Azhdam et al., 2020). For the average eyes, this would translate to 59.58 ng MPA in females and 63.68 ng MPA in males to be injected into the vitreous body to reach a concentration of 40 µM. As deviations of the average VCV are common, an individual value could be assessed before injection. The actual VCV can be calculated using high-resolution computer tomography of the eye. The amount of solvent should be kept to a minimum, as the maximum safe volume to be injected is 100-200 µl, with higher volumes increasing the intraocular pressure exponentially, potentially provoking the necessity of a pressure-relieving paracentesis (Allmendinger et al., 2021). As the vitreous body is barrier surrounded, injected substances will stay in this space and remain active for a longer period of time compared to regular blood stream distribution. The elimination of active ingredients depends on the molecular size and degree of lipophilicity.

For systemic oral application, it is necessary to mention, that while we used MPA in our experiments, Yang's group used MMF. Without consideration of the BRB and with uniform distribution of the active substance an oral dose of 500 mg would reach a blood stream concentration of approximately 40 µM. With a half time of MMF of 16 hours, one 500 mg dose daily may be used as a maintenance dose. Considering the properties of the BRB, such as permeability though, concentration in the retina and specifically the photoreceptors would most likely be much lower. Since it is currently not known how much MMF would pass through the

BRB, it is not possible to say exactly how high a systemic dose must be to cause an effect there.

Aside from aspects facilitating clinical studies, more knowledge concerning fundamental pathways and questions are needed: Prolonged explant cultures with read-outs on cone survivability after rod cell rescue are needed to estimate high-resolution cone-dependent sight in a prognostic manner.

Different mouse models (based of different mutations affecting the downstream IMPDH1 and cGMP pathway) like *Pde6a* mutants or a more slowly progressing model, such as *rd2* or *rd10* mice, may give further insights into pathways and their transferability across different disease-causing mutations.

Taken together, with research on RP pathomechanisms and treatment options being an active field, this work adds to the knowledge about RP pathology in *rd1* animals and supports MPA as a potential future treatment.

5 Summary

Purpose: Retinitis pigmentosa is a degenerative genetic disorder in which photoreceptor cell death can be connected to high cGMP levels. This is exemplified by the *rd1* mouse model where a mutation in the *Pde6b* gene leads to decreased cGMP hydrolysis in photoreceptors. While the enzyme guanylyl cyclase (GC) synthesizes cGMP in photoreceptors, inosine monophosphate dehydrogenase-1 (IMPDH1) catalyzes the rate-limiting step in the biosynthesis leading up to cGMP. Hence, inhibiting IMPDH1 may be a strategy for the reduction of photoreceptor cGMP levels and cell death. I explored the capacity of the registered immunosuppressive drug mycophenolic acid (MPA) to reduce photoreceptor cGMP levels and cell death in *rd1* retinal explant cultures.

Methods: The retinal expression patterns of IMPDH1 and GC were assessed in wild-type and *rd1* mouse retina using immunofluorescence. Organotypic retinal explant cultures derived from post-natal day (P) 5 *rd1* mice were treated with MPA in six different concentrations ranging from 1 to 1000 µM. Parallel control cultures received vehicle or medium only. The retinal explants were cultured from P5 to P11 with medium changes every two days. At P11, the explants were fixed in paraformaldehyde, cryosectioned, and stained for cell death using the TUNEL-assay. TUNEL-positive cells were counted and compared with controls. To determine treatment effects on cone photoreceptors, these were quantified using PNA labelling.

Results: IMPDH1 was expressed in photoreceptor inner segments, outer plexiform layer, neurites in the outer nuclear layer, and cell bodies in the inner nuclear layer. GC staining labelled the outer segments of photoreceptors. In *rd1 ex vivo* explant cultures treated with MPA, cell death decreased in a concentration-dependent manner. Between 40 and 250 µM cell death was significantly reduced, while at 1000 µM cell death was strongly increased, and retinal structure was lost. No significant differences in cone cell numbers were found by PNA staining.

Conclusion: The localization of IMPDH1 expression to photoreceptor inner segments makes it a potentially druggable target for the treatment of retinitis pigmentosa. Importantly, the treatment with MPA revealed a neuroprotective effect in a concentration range achievable in a clinical setting.

5.1 Zusammenfassung

Ziel: Retinitis Pigmentosa ist eine erbliche degenerative Erkrankung, bei der der Zelltod von Photorezeptoren mit einem hohen cGMP-Spiegel in Verbindung gebracht wird. Ein Beispiel hierfür ist das *rd1*-Mausmodell, bei dem eine Mutation im *Pde6b*-Gen zu einer verminderten cGMP-Hydrolyse in Photorezeptoren führt. Während die Guanylatzyklase (GC) cGMP in den Photorezeptoren synthetisiert, katalysiert das Enzym Inosinmonophosphat-Dehydrogenase 1 (IMPDH1) den geschwindigkeits-bestimmenden Schritt in der *de-novo* Biosynthese von Guanosinmonophosphat, welche letztlich zu cGMP führt. Daher könnte die Hemmung von IMPDH1 eine Strategie zur Verringerung des cGMP-Spiegels und des Zelltods in Photorezeptoren sein. Ich habe untersucht, inwieweit das zugelassene Immunsuppressivum Mycophenolsäure den Zelltod der Photorezeptoren in *rd1*-Netzhautexplantatkulturen verringern kann.

Methoden: Das retinale Expressionsmuster von IMPDH1 und GC wurde in der Netzhaut von Wildtyp- und *rd1*-Mäusen mittels Immunfluoreszenzfärbungen untersucht. Anschließend wurden am post-natalen Tag (P) 5 organotypische Netzhaut-Explantatkulturen von *rd1*-Mäusen erstellt und mit MPA in sechs verschiedenen Konzentrationen zwischen 1 und 1000 µM behandelt. Parallellaufende Kontrollkulturen erhielten nur Vehikel oder Medium. Die Netzhautexplantate wurden von P5 bis P11 kultiviert, das Medium wurde alle zwei Tage gewechselt. An P11 wurden die Explantate in Paraformaldehyd fixiert, am Kryotom geschnitten und mit dem TUNEL-Assay auf Zelltod angefärbt. Die TUNEL-positiven Zellen wurden manuell gezählt und mit den Kontrollen verglichen. Um die Wirkung von MPA auf die Zapfen zu erheben, wurden diese mit Hilfe von *peanut agglutinin* (PNA) gefärbt und quantifiziert.

Ergebnisse: IMPDH1 wurde in den inneren Segmenten der Photorezeptoren, der äußeren plexiformen Schicht, den Neuriten in der äußeren Kernschicht und den Zellkörpern in der inneren Kernschicht exprimiert. Die GC-Färbung markierte die äußeren Segmente der Photorezeptoren. In *rd1 ex vivo* Explantatkulturen, die mit MPA behandelt wurden, verringerte sich der Zelltod konzentrationsabhängig. Konzentrationen von 40 bis 250 µM reduzierten den Zelltod signifikant. Bei 1000

µM war der Zelltod jedoch stark erhöht, und die Netzhautstruktur ging verloren. Die Quantifizierung der PNA-Färbungen zeigte keinen signifikanten Unterschied in der Anzahl der Zapfen.

Fazit: Die Lokalisierung der IMPDH1-Expression in den inneren Segmenten der Photorezeptoren macht sie zu einem potenziellen Angriffspunkt für die Behandlung von Retinitis Pigmentosa. Die Behandlung mit MPA in Explantatkulturen der Netzhaut zeigte einen neuroprotektiven Effekt in einer Konzentrationsspanne, die auch im klinischen Rahmen darstellbar ist.

6 Annex

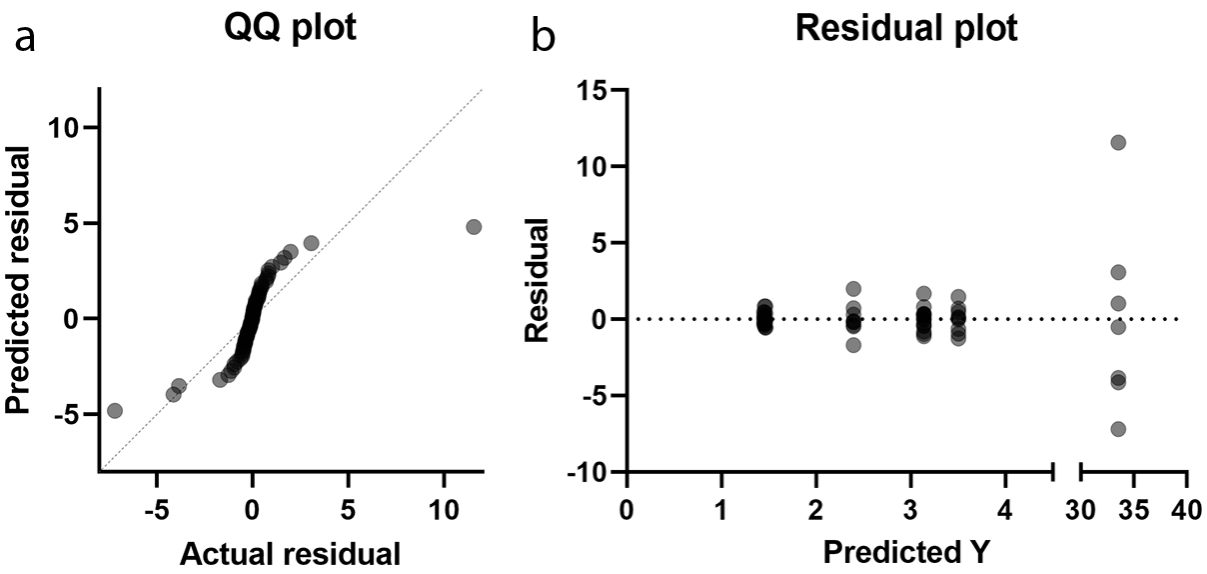

Figure 19: QQ plot and Residual plot of TUNEL positive cell % comparison

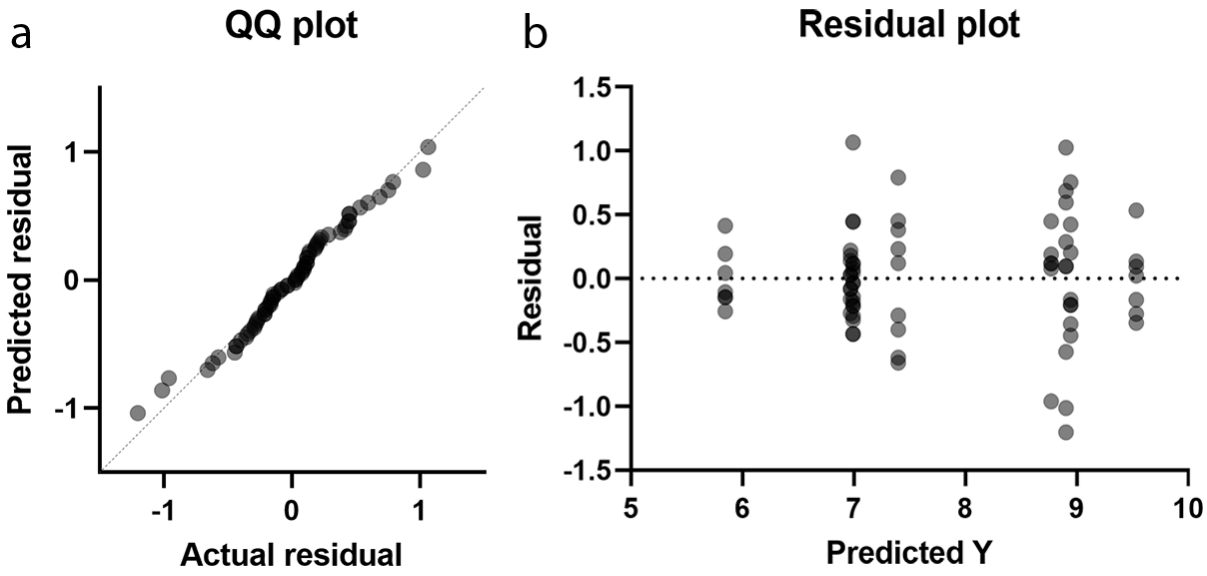

Figure 20: QQ plot and Residual Plot of ONL photoreceptor row count comparison

Table 6: Individual values and descriptive statistics for TUNEL positive cells, in vivo retina

Individual values (multiple sections of the same eyes averaged) and descriptive statistics of in vivo rd1 and WT P11 animals. Wild type (WT), postnatal day (P).

	WT	***rd1***
Individual values ↓	0.04	5.64
	0.08	5.61
	0.06	5.81
Number of values	3	3
Minimum	0.04	5.61
Maximum	0.08	5.81
Range	0.04	0,2
Mean	0.06	5.69
Std. Deviation	0.02	0.11
Std. Error of Mean	0.01	0.06

Table 7: Data for DMSO and CM controls

Individual values (multiple sections of the same explant averaged) and descriptive statistics of P11 ex vivo explant cultures after treatment. Dimethyl sulfoxide (DMSO), complete medium (CM), postnatal day (P).

	Number of photoreceptor rows		**TUNEL+ cells in %**	
	DMSO	**CM**	**DMSO**	**CM**
Individual values ↓	7.44	7.07	2.03	3.95
	8.06	6.78	2.18	3.48
	6.81	7.44	3.16	3.49
	7.11	6.67	2.33	3.44
	6.96	7.11	3.13	3.29
	6.85	6.56	3.22	2.87
	6.7	7.04	3.14	2.74
	6.96	6.56	4.81	3.42
	6.78		2.7	
No. of retinal explants	9	8	9	8
Minimum	6.7	6.56	2.03	2.74
Maximum	8.06	7.44	4.81	3.95
Range	1.36	0.88	2.78	1.21
Mean	7.07	6.90	2.97	3.34
Std. Deviation	0.43	0.31	0.83	0.38
Std. Error of Mean	0.14	0.11	0.28	0.14

Table 8: Data for TUNEL positive cells in retinal explants

Individual values (multiple sections of the same explant averaged) and descriptive statistics of P11 ex vivo explant cultures after treatment. Wild type (WT), Mycophenolic acid (MPA), postnatal day (P).

	WT	Control	1 µM MPA	10 µM MPA	40 µM MPA	78 µM MPA	250 µM MPA	1000 µM MPA
Individual values ↓	0.125	2.03	2.24	2.22	2.3	1	1.34	45.13
	1.17	2.18	2.87	2.7	1.84	1.31	1.92	36.62
	0.83	3.16	3.5	2.28	1.41	1.11	1.63	33.04
	1.3	2.33	2.56	0.7	1.38	1.15	1.55	34.57
	1.21	3.13	3.64	2.02	0.92	1.52	1.42	26.35
	0.44	3.22	4.21	1.93	0.94	2.29	1.49	29.71
	0.87	3.14	3.57	3.12		1.91	1.17	29.42
		4.81	4.98	2.2		1.63	1.08	
		2.7	3.98	4.39		1.19		
		3.95						
		3.48						
		3.49						
		3.44						
		3.29						
		2.87						
		2.74						
		3.42						
No. of retinal explants	7	17	9	9	6	9	8	7
Minimum	0.13	2.03	2.24	0.7	0.92	1	1.08	26.35
Maximum	1.3	4.81	4.98	4.39	2.3	2.29	1.92	45.13
Range	1.18	2.78	2.74	3.69	1.38	1.29	0.84	18.78
Mean	0.85	3.14	3.51	2.40	1.47	1.46	1.45	33.55
Std. Deviation	0.43	0.67	0.85	0.99	0.53	0.43	0.27	6.17
Std. Error of Mean	0.16	0.16	0.28	0.33	0.22	0.14	0.09	2.33

Table 9: Data for ONL photoreceptor rows in retinal explants

Individual values (multiple sections of the same explant averaged) and descriptive statistics of P11 ex vivo explant cultures after treatment. Wild type (WT), Mycophenolic acid (MPA), postnatal day (P).

	WT	Control	1 µM MPA	10 µM MPA	40 µM MPA	78 µM MPA	250 µM MPA	1000 µM MPA
Individual values ↓	9.26	7,44	7,11	8,19	7,81	9,59	8,78	5,89
	9.67	8.06	7.19	7.85	8.96	9	9.7	6.26
	9.56	6.81	7	7.63	8.89	9	8.5	6.04
	10.07	7.11	7.15	7.11	8.85	9.5	8.59	5.74
	9.19	6.96	6.89	7.78	9.22	7.7	8.74	5.7
	9.63	6.85	6.7	7	8.89	9.19	8.74	5.59
	9.37	6.7	6.81	6.78		7.89	9.37	5.7
		6.96	7	6.74		9.93	9.15	
		6.78	6.89	7.52		8.33		
		7.07						
		6.78						
		7.44						
		6.67						
		7.11						
		6.56						
		7.04						
		6.56						
No. of retinal explants	7	17	9	9	6	9	8	7
Minimum	9.19	6.56	6.7	6.74	7.81	7.7	8.5	5.59
Maximum	10.07	8.06	7.19	8.19	9.22	9.93	9.7	6.26
Range	0.88	1.5	0.49	1.45	1.41	2.23	1.2	0.67
Mean	9.54	6.99	6.97	7.4	8.77	8.90	8.95	5.85
Std. Deviation	0.31	0.38	0.16	0.51	0.49	0.77	0.42	0.24
Std. Error of Mean	0.11	0.09	0.05	0.17	0.20	0.26	0.15	0.09

Table 10: Data for Peanut agglutinin-stained cones

Individual values (multiple sections of the same explant averaged) and descriptive statistics of P11 ex vivo explant cultures after treatment. Wild type (WT), Dimethyl sulfoxide (DMSO), Mycophenolic acid (MPA), postnatal day (P).

	WT	DMSO	40 µM MPA
Individual values ↓	9.03	8.16	7.06
	6.53	6.34	6.71
	6.38	7.56	7.55
	7.05	8.27	5.82
	5.64	4.99	6.51
	7.79	8.59	6.27
	5.56		
No. of retinal explants	7	6	6
Minimum	5.56	4.99	5.82
Maximum	9.03	8.59	7.55
Range	3.47	3.6	1.73
Mean	6.85	7.32	6.65
Std. Deviation	1.23	1.39	0.61
Std. Error of Mean	0.47	0.57	0.25

7 Bibliography

AGRAHARI, V., MANDAL, A., AGRAHARI, V., TRINH, H. M., JOSEPH, M., RAY, A., HADJI, H., MITRA, R., PAL, D. & MITRA, A. K. 2016. A comprehensive insight on ocular pharmacokinetics. *Drug Deliv Transl Res,* 6**,** 735-754.

AGRAWAL, S. A., BURGOYNE, T., EBLIMIT, A., BELLINGHAM, J., PARFITT, D. A., LANE, A., NICHOLS, R., ASOMUGHA, C., HAYES, M. J., MUNRO, P. M., XU, M., WANG, K., FUTTER, C. E., LI, Y., CHEN, R. & CHEETHAM, M. E. 2017. REEP6 deficiency leads to retinal degeneration through disruption of ER homeostasis and protein trafficking. *Hum Mol Genet,* 26**,** 2667-2677.

AHERNE, A., KENNAN, A., KENNA, P. F., MCNALLY, N., LLOYD, D. G., ALBERTS, I. L., KIANG, A. S., HUMPHRIES, M. M., AYUSO, C., ENGEL, P. C., GU, J. J., MITCHELL, B. S., FARRAR, G. J. & HUMPHRIES, P. 2004. On the molecular pathology of neurodegeneration in IMPDH1-based retinitis pigmentosa. *Hum Mol Genet,* 13**,** 641-50.

ALLISON, A. C., KOWALSKI, W. J., MULLER, C. D. & EUGUI, E. M. 1993. Mechanisms of action of mycophenolic acid. *Ann N Y Acad Sci,* 696**,** 63-87.

ALLMENDINGER, A., BUTT, Y. L. & MUELLER, C. 2021. Intraocular pressure and injection forces during intravitreal injection into enucleated porcine eyes. *Eur J Pharm Biopharm,* 166**,** 87-93.

ALPERN, M., FULTON, A. B. & BAKER, B. N. 1987. "Self-screening" of rhodopsin in rod outer segments. *Vision Res,* 27**,** 1459-70.

ARANGO-GONZALEZ, B., TRIFUNOVIC, D., SAHABOGLU, A., KRANZ, K., MICHALAKIS, S., FARINELLI, P., KOCH, S., KOCH, F., COTTET, S., JANSSEN-BIENHOLD, U., DEDEK, K., BIEL, M., ZRENNER, E., EULER, T., EKSTROM, P., UEFFING, M. & PAQUET-DURAND, F. 2014. Identification of a common non-apoptotic cell death mechanism in hereditary retinal degeneration. *PLoS One,* 9**,** e112142.

ARSHAVSKY, V. Y., LAMB, T. D. & PUGH, E. N., JR. 2002. G proteins and phototransduction. *Annu Rev Physiol,* 64**,** 153-87.

AUGHEY, G. N. & LIU, J. L. 2015. Metabolic regulation via enzyme filamentation. *Crit Rev Biochem Mol Biol,* 51**,** 282-93.

AZHDAM, A. M., GOLDBERG, R. A. & UGRADAR, S. 2020. In Vivo Measurement of the Human Vitreous Chamber Volume Using Computed Tomography Imaging of 100 Eyes. *Transl Vis Sci Technol,* 9**,** 2.

BELHADJ, S., TOLONE, A., CHRISTENSEN, G., DAS, S., CHEN, Y. & PAQUET-DURAND, F. 2020. Long-Term, Serum-Free Cultivation of Organotypic Mouse Retina Explants with Intact Retinal Pigment Epithelium. *J Vis Exp*.

BIRNGRUBER, T., RAML, R., GLADDINES, W., GATSCHELHOFER, C., GANDER, E., GHOSH, A., KROATH, T., GAILLARD, P. J., PIEBER, T. R. & SINNER, F. 2014. Enhanced doxorubicin delivery to the brain administered through glutathione PEGylated liposomal doxorubicin (2B3-101) as compared with generic Caelyx,((R))/Doxil((R))--a cerebral open flow microperfusion pilot study. *J Pharm Sci,* 103**,** 1945-1948.

BLANKS, J. C. & JOHNSON, L. V. 1984. Specific binding of peanut lectin to a class of retinal photoreceptor cells. A species comparison. *Invest Ophthalmol Vis Sci,* 25**,** 546-57.

BOHLEY, M., DILLINGER, A. E., TAMM, E. R. & GOEPFERICH, A. 2022. Targeted drug delivery to the retinal pigment epithelium: Untapped therapeutic potential for retinal diseases. *Drug Discov Today,* 27**,** 2497-2509.

BOUGHMAN, J. A., CONNEALLY, P. M. & NANCE, W. E. 1980. Population genetic studies of retinitis pigmentosa. *Am J Hum Genet,* 32**,** 223-35.

BOWES, C., LI, T., DANCIGER, M., BAXTER, L. C., APPLEBURY, M. L. & FARBER, D. B. 1990. Retinal degeneration in the rd mouse is caused by a defect in the beta subunit of rod cGMP-phosphodiesterase. *Nature,* 347**,** 677-80.

BOWNE, S. J., LIU, Q., SULLIVAN, L. S., ZHU, J., SPELLICY, C. J., RICKMAN, C. B., PIERCE, E. A. & DAIGER, S. P. 2006. Why do mutations in the ubiquitously expressed housekeeping gene IMPDH1 cause retina-specific photoreceptor degeneration? *Invest Ophthalmol Vis Sci,* 47**,** 3754-65.

BOWNE, S. J., SULLIVAN, L. S., BLANTON, S. H., CEPKO, C. L., BLACKSHAW, S., BIRCH, D. G., HUGHBANKS-WHEATON, D., HECKENLIVELY, J. R. & DAIGER, S. P. 2002. Mutations in the inosine monophosphate dehydrogenase 1 gene (IMPDH1) cause the RP10 form of autosomal dominant retinitis pigmentosa. *Hum Mol Genet,* 11**,** 559-68.

BULLINGHAM, R. E., NICHOLLS, A. J. & KAMM, B. R. 1998. Clinical pharmacokinetics of mycophenolate mofetil. *Clin Pharmacokinet,* 34**,** 429-55.

BURRELL, A. L. & KOLLMAN, J. M. 2022. IMPDH dysregulation in disease: a mini review. *Biochem Soc Trans,* 50**,** 71-82.

BUSH, R. A., KONONEN, L., MACHIDA, S. & SIEVING, P. A. 2000. The effect of calcium channel blocker diltiazem on photoreceptor degeneration in the rhodopsin Pro213His rat. *Invest Ophthalmol Vis Sci,* 41**,** 2697-701.

CAFFE, A. R., SODERPALM, A. & VAN VEEN, T. 1993. Photoreceptor-specific protein expression of mouse retina in organ culture and retardation of rd degeneration in vitro by a combination of basic fibroblast and nerve growth factors. *Curr Eye Res,* 12**,** 719-26.

CARTER-DAWSON, L. D., LAVAIL, M. M. & SIDMAN, R. L. 1978. Differential effect of the rd mutation on rods and cones in the mouse retina. *Invest Ophthalmol Vis Sci,* 17**,** 489-98.

CEPKO, C. L., AUSTIN, C. P., YANG, X., ALEXIADES, M. & EZZEDDINE, D. 1996. Cell fate determination in the vertebrate retina. *Proc Natl Acad Sci U S A,* 93**,** 589-95.

CHANG, B., HAWES, N. L., HURD, R. E., DAVISSON, M. T., NUSINOWITZ, S. & HECKENLIVELY, J. R. 2002. Retinal degeneration mutants in the mouse. *Vision Res,* 42**,** 517-25.

CHANG, C. C., LIN, W. C., PAI, L. M., LEE, H. S., WU, S. C., DING, S. T., LIU, J. L. & SUNG, L. Y. 2015. Cytoophidium assembly reflects upregulation of IMPDH activity. *J Cell Sci,* 128**,** 3550-5.

CHANG, D. T., HERCEG, M. C., BILONICK, R. A., CAMEJO, L., SCHUMAN, J. S. & NOECKER, R. J. 2009. Intracameral dexamethasone reduces

inflammation on the first postoperative day after cataract surgery in eyes with and without glaucoma. *Clin Ophthalmol,* 3**,** 345-55.

CHANG, G. Q., HAO, Y. & WONG, F. 1993. Apoptosis: final common pathway of photoreceptor death in rd, rds, and rhodopsin mutant mice. *Neuron,* 11**,** 595-605.

CHOUDHURY, S., BHOOTADA, Y., GORBATYUK, O. & GORBATYUK, M. 2013. Caspase-7 ablation modulates UPR, reprograms TRAF2-JNK apoptosis and protects T17M rhodopsin mice from severe retinal degeneration. *Cell Death Dis,* 4**,** e528.

CHRISTENSEN, G., CHEN, Y., URIMI, D., ZIZMARE, L., TRAUTWEIN, C., SCHIPPER, N. & PAQUET-DURAND, F. 2023. Pyruvate-conjugation of PEGylated liposomes for targeted drug delivery to retinal photoreceptors. *Biomed Pharmacother,* 163**,** 114717.

CLEGHORN, W. M., BURRELL, A. L., GIARMARCO, M. M., BROCK, D. C., WANG, Y., CHAMBERS, Z. S., DU, J., KOLLMAN, J. M. & BROCKERHOFF, S. E. 2022. A highly conserved zebrafish IMPDH retinal isoform produces the majority of guanine and forms dynamic protein filaments in photoreceptor cells. *J Biol Chem,* 298**,** 101441.

CROSS, N., VAN STEEN, C., ZEGAOUI, Y., SATHERLEY, A. & ANGELILLO, L. 2022. Current and Future Treatment of Retinitis Pigmentosa. *Clin Ophthalmol,* 16**,** 2909-2921.

DA VIOLANTE, G., ZERROUK, N., RICHARD, I., PROVOT, G., CHAUMEIL, J. C. & ARNAUD, P. 2002. Evaluation of the cytotoxicity effect of dimethyl sulfoxide (DMSO) on Caco2/TC7 colon tumor cell cultures. *Biol Pharm Bull,* 25**,** 1600-3.

DAIGER, S. P., ROSSITER, B. J. F., GREENBERG, J., CHRISTOFFELS, A. & HIDE, W. 2024. *RetNet, the Retinal Information Network* [Online]. Available: https://web.sph.uth.edu/RetNet/ [Accessed July 12 2024].

DALMARCO, E. M., BUDNI, P., PARISOTTO, E. B., WILHELM FILHO, D. & FRODE, T. S. 2009. Antioxidant effects of mycophenolate mofetil in a murine pleurisy model. *Transpl Immunol,* 22**,** 12-7.

DANIEL, E., THORNE, J. E., NEWCOMB, C. W., PUJARI, S. S., KACMAZ, R. O., LEVY-CLARKE, G. A., NUSSENBLATT, R. B., ROSENBAUM, J. T., SUHLER, E. B., FOSTER, C. S., JABS, D. A. & KEMPEN, J. H. 2010. Mycophenolate mofetil for ocular inflammation. *Am J Ophthalmol,* 149**,** 423-32 e1-2.

DE ABREU COSTA, L., HENRIQUE FERNANDES OTTONI, M., DOS SANTOS, M. G., MEIRELES, A. B., GOMES DE ALMEIDA, V., DE FATIMA PEREIRA, W., ALVES DE AVELAR-FREITAS, B. & EUSTAQUIO ALVIM BRITO-MELO, G. 2017. Dimethyl Sulfoxide (DMSO) Decreases Cell Proliferation and TNF-alpha, IFN-gamma, and IL-2 Cytokines Production in Cultures of Peripheral Blood Lymphocytes. *Molecules,* 22.

DEHGHANI, F., HISCHEBETH, G. T., WIRJATIJASA, F., KOHL, A., KORF, H. W. & HAILER, N. P. 2003. The immunosuppressant mycophenolate mofetil attenuates neuronal damage after excitotoxic injury in hippocampal slice cultures. *Eur J Neurosci,* 18**,** 1061-72.

DEHGHANI, F., SAYAN, M., CONRAD, A., EVERS, J., GHADBAN, C., BLAHETA, R., KORF, H. W. & HAILER, N. P. 2010. Inhibition of microglial

and astrocytic inflammatory responses by the immunosuppressant mycophenolate mofetil. *Neuropathol Appl Neurobiol,* 36**,** 598-611.

DEL AMO, E. M., RIMPELA, A. K., HEIKKINEN, E., KARI, O. K., RAMSAY, E., LAJUNEN, T., SCHMITT, M., PELKONEN, L., BHATTACHARYA, M., RICHARDSON, D., SUBRIZI, A., TURUNEN, T., REINISALO, M., ITKONEN, J., TOROPAINEN, E., CASTELEIJN, M., KIDRON, H., ANTOPOLSKY, M., VELLONEN, K. S., RUPONEN, M. & URTTI, A. 2017. Pharmacokinetic aspects of retinal drug delivery. *Prog Retin Eye Res,* 57**,** 134-185.

DEMETRIUS, L. 2005. Of mice and men. When it comes to studying ageing and the means to slow it down, mice are not just small humans. *EMBO Rep,* 6 Spec No**,** S39-44.

DEN HOLLANDER, A. I., ROEPMAN, R., KOENEKOOP, R. K. & CREMERS, F. P. 2008. Leber congenital amaurosis: genes, proteins and disease mechanisms. *Prog Retin Eye Res,* 27**,** 391-419.

DIZHOOR, A. M. & PESHENKO, I. V. 2021. Regulation of retinal membrane guanylyl cyclase (RetGC) by negative calcium feedback and RD3 protein. *Pflugers Arch,* 473**,** 1393-1410.

DORMEGNY, L., STUDER, F., SAUER, A., BALLONZOLI, L., SPEEG-SCHATZ, C., BOURCIER, T., DOLLFUS, H. & GAUCHER, D. 2024. Could internal limiting membrane peeling before Voretigen neparvovec-ryzl subretinal injection prevent focal chorioretinal atrophy? *Heliyon,* 10**,** e25154.

ETTINGER, M. P., LITTLEJOHN, T. W., SCHWARTZ, S. L., WEISS, S. R., MCILWAIN, H. H., HEYMSFIELD, S. B., BRAY, G. A., ROBERTS, W. G., HEYMAN, E. R., STAMBLER, N., HESHKA, S., VICARY, C. & GULER, H. P. 2003. Recombinant variant of ciliary neurotrophic factor for weight loss in obese adults: a randomized, dose-ranging study. *JAMA,* 289**,** 1826-32.

FARBER, D. B. & LOLLEY, R. N. 1974. Cyclic guanosine monophosphate: elevation in degenerating photoreceptor cells of the C3H mouse retina. *Science,* 186**,** 449-51.

FRASSON, M., SAHEL, J. A., FABRE, M., SIMONUTTI, M., DREYFUS, H. & PICAUD, S. 1999. Retinitis pigmentosa: rod photoreceptor rescue by a calcium-channel blocker in the rd mouse. *Nat Med,* 5**,** 1183-7.

GAVRIELI, Y., SHERMAN, Y. & BEN-SASSON, S. A. 1992. Identification of programmed cell death in situ via specific labeling of nuclear DNA fragmentation. *J Cell Biol,* 119**,** 493-501.

GEORGIOU, M., FUJINAMI, K. & MICHAELIDES, M. 2021. Inherited retinal diseases: Therapeutics, clinical trials and end points-A review. *Clin Exp Ophthalmol,* 49**,** 270-288.

GERMER, A., JAHNKE, C., MACK, A., ENZMANN, V. & REICHENBACH, A. 1997. Modification of glutamine synthetase expression by mammalian Muller (glial) cells in retinal organ cultures. *Neuroreport,* 8**,** 3067-72.

GRASL-KRAUPP, B., RUTTKAY-NEDECKY, B., KOUDELKA, H., BUKOWSKA, K., BURSCH, W. & SCHULTE-HERMANN, R. 1995. In situ detection of fragmented DNA (TUNEL assay) fails to discriminate among apoptosis, necrosis, and autolytic cell death: a cautionary note. *Hepatology,* 21**,** 1465-8.

GROSSMAN, R., FOX, L. E., GOROVITS, R., BEN-DROR, I., REISFELD, S. & VARDIMON, L. 1994. Molecular basis for differential expression of glutamine synthetase in retina glia and neurons. *Brain Res Mol Brain Res,* 21**,** 312-20.

HAMEL, C. 2006. Retinitis pigmentosa. *Orphanet J Rare Dis,* 1**,** 40.

HAO, Q. & BAILEY, S. 2023. *Anti-Vascular Endothelial Growth Factor Drugs for Age-Related Macular Degeneration: CADTH Health Technology Review.* Ottawa (ON).

HE, X., SMEETS, R. L., KOENEN, H. J., VINK, P. M., WAGENAARS, J., BOOTS, A. M. & JOOSTEN, I. 2011. Mycophenolic acid-mediated suppression of human CD4+ T cells: more than mere guanine nucleotide deprivation. *Am J Transplant,* 11**,** 439-49.

HEDSTROM, L. 2009. IMP dehydrogenase: structure, mechanism, and inhibition. *Chem Rev,* 109**,** 2903-28.

HIMAWAN, E., EKSTROM, P., BUZGO, M., GAILLARD, P., STEFANSSON, E., MARIGO, V., LOFTSSON, T. & PAQUET-DURAND, F. 2019. Drug delivery to retinal photoreceptors. *Drug Discov Today,* 24**,** 1637-1643.

JIAO, K., SAHABOGLU, A., ZRENNER, E., UEFFING, M., EKSTROM, P. A. & PAQUET-DURAND, F. 2016. Efficacy of PARP inhibition in Pde6a mutant mouse models for retinitis pigmentosa depends on the quality and composition of individual human mutations. *Cell Death Discov,* 2**,** 16040.

JOHNSON, K. S. & CHU, D. S. 2010. Evaluation of sub-Tenon triamcinolone acetonide injections in the treatment of scleritis. *Am J Ophthalmol,* 149**,** 77-81.

JONES, R. B., WALSH, M. & SMITH, K. G. 2009. What is the value of mycophenolate mofetil as induction and maintenance therapy in lupus nephritis? *Curr Opin Rheumatol,* 21**,** 256-61.

KARLSSON, M., ZHANG, C., MEAR, L., ZHONG, W., DIGRE, A., KATONA, B., SJOSTEDT, E., BUTLER, L., ODEBERG, J., DUSART, P., EDFORS, F., OKSVOLD, P., VON FEILITZEN, K., ZWAHLEN, M., ARIF, M., ALTAY, O., LI, X., OZCAN, M., MARDINOGLU, A., FAGERBERG, L., MULDER, J., LUO, Y., PONTEN, F., UHLEN, M. & LINDSKOG, C. 2021. A single-cell type transcriptomics map of human tissues. *Sci Adv,* 7.

KEELER, C. E. 1924. The Inheritance of a Retinal Abnormality in White Mice. *Proc Natl Acad Sci U S A,* 10**,** 329-33.

KENNAN, A., AHERNE, A., BOWNE, S. J., DAIGER, S. P., FARRAR, G. J., KENNA, P. F. & HUMPHRIES, P. 2003. On the role of IMPDH1 in retinal degeneration. *Adv Exp Med Biol,* 533**,** 13-8.

KEPPEKE, G. D., CHANG, C. C., PENG, M., CHEN, L. Y., LIN, W. C., PAI, L. M., ANDRADE, L. E. C., SUNG, L. Y. & LIU, J. L. 2018. IMP/GTP balance modulates cytoophidium assembly and IMPDH activity. *Cell Div,* 13**,** 5.

KOENEKOOP, R. K. 2008. Successful RPE65 gene replacement and improved visual function in humans. *Ophthalmic Genet,* 29**,** 89-91.

KOO, H., MOON, H., HAN, H., NA, J. H., HUH, M. S., PARK, J. H., WOO, S. J., PARK, K. H., KWON, I. C., KIM, K. & KIM, H. 2012. The movement of self-assembled amphiphilic polymeric nanoparticles in the vitreous and retina after intravitreal injection. *Biomaterials,* 33**,** 3485-93.

KULKARNI, M., TRIFUNOVIC, D., SCHUBERT, T., EULER, T. & PAQUET-DURAND, F. 2016. Calcium dynamics change in degenerating cone photoreceptors. *Hum Mol Genet,* 2**5,** 3729-3740.

LAVAIL, M. M., YASUMURA, D., MATTHES, M. T., LAU-VILLACORTA, C., UNOKI, K., SUNG, C. H. & STEINBERG, R. H. 1998. Protection of mouse photoreceptors by survival factors in retinal degenerations. *Invest Ophthalmol Vis Sci,* 39**,** 592-602.

LIU, J. L. 2010. Intracellular compartmentation of CTP synthase in Drosophila. *J Genet Genomics,* 37**,** 281-96.

MAURICE, D. 2001. Review: practical issues in intravitreal drug delivery. *J Ocul Pharmacol Ther,* 17**,** 393-401.

MOISEYEV, G., CHEN, Y., TAKAHASHI, Y., WU, B. X. & MA, J. X. 2005. RPE65 is the isomerohydrolase in the retinoid visual cycle. *Proc Natl Acad Sci U S A,* 102**,** 12413-8.

MOSHIRI, A. 2021. Animals Models of Inherited Retinal Disease. *Int Ophthalmol Clin,* 61**,** 113-130.

MURAKAMI, Y., IKEDA, Y., NAKATAKE, S., MILLER, J. W., VAVVAS, D. G., SONODA, K. H. & ISHIBASHI, T. 2015. Necrotic cone photoreceptor cell death in retinitis pigmentosa. *Cell Death Dis,* 6**,** e2038.

NEWTON, F. & MEGAW, R. 2020. Mechanisms of Photoreceptor Death in Retinitis Pigmentosa. *Genes (Basel),* 11.

OBOLENSKY, A., BERENSHTEIN, E., LEDERMAN, M., BULVIK, B., ALPER-PINUS, R., YAUL, R., DELEON, E., CHOWERS, I., CHEVION, M. & BANIN, E. 2011. Zinc-desferrioxamine attenuates retinal degeneration in the rd10 mouse model of retinitis pigmentosa. *Free Radic Biol Med,* 51**,** 1482-91.

OKADA, A. A., WAKABAYASHI, T., MORIMURA, Y., KAWAHARA, S., KOJIMA, E., ASANO, Y. & HIDA, T. 2003. Trans-Tenon's retrobulbar triamcinolone infusion for the treatment of uveitis. *Br J Ophthalmol,* 87**,** 968-71.

PANACKEL, C., MATHEW, J. F., FAWAS, N. M. & JACOB, M. 2022. Immunosuppressive Drugs in Liver Transplant: An Insight. *J Clin Exp Hepatol,* 12**,** 1557-1571.

PAPADIMITRIOU, J. C., CANGRO, C. B., LUSTBERG, A., KHALED, A., NOGUEIRA, J., WILAND, A., RAMOS, E., KLASSEN, D. K. & DRACHENBERG, C. B. 2003. Histologic features of mycophenolate mofetil-related colitis: a graft-versus-host disease-like pattern. *Int J Surg Pathol,* 11**,** 295-302.

PAQUET-DURAND, F., BECK, S., MICHALAKIS, S., GOLDMANN, T., HUBER, G., MUHLFRIEDEL, R., TRIFUNOVIC, D., FISCHER, M. D., FAHL, E., DUETSCH, G., BECIROVIC, E., WOLFRUM, U., VAN VEEN, T., BIEL, M., TANIMOTO, N. & SEELIGER, M. W. 2011. A key role for cyclic nucleotide gated (CNG) channels in cGMP-related retinitis pigmentosa. *Hum Mol Genet,* 20**,** 941-7.

PAQUET-DURAND, F., HAUCK, S. M., VAN VEEN, T., UEFFING, M. & EKSTROM, P. 2009. PKG activity causes photoreceptor cell death in two retinitis pigmentosa models. *J Neurochem,* 108**,** 796-810.

PAQUET-DURAND, F., SILVA, J., TALUKDAR, T., JOHNSON, L. E., AZADI, S., VAN VEEN, T., UEFFING, M., HAUCK, S. M. & EKSTROM, P. A. 2007.

Excessive activation of poly(ADP-ribose) polymerase contributes to inherited photoreceptor degeneration in the retinal degeneration 1 mouse. *J Neurosci,* 27**,** 10311-9.

PLANA-BONAMAISO, A., LOPEZ-BEGINES, S., FERNANDEZ-JUSTEL, D., JUNZA, A., SOLER-TAPIA, A., ANDILLA, J., LOZA-ALVAREZ, P., ROSA, J. L., MIRALLES, E., CASALS, I., YANES, O., DE LA VILLA, P., BUEY, R. M. & MENDEZ, A. 2020. Post-translational regulation of retinal IMPDH1 in vivo to adjust GTP synthesis to illumination conditions. *Elife,* 9.

PROTEINATLAS.ORG, H. P. A. *Human Protein Atlas proteinatlas.org* [Online]. Available: https://www.proteinatlas.org/ENSG00000106348-IMPDH1/single+cell+type/eye [Accessed 24. April 2024].

QI, W., DING, D. & SALVI, R. J. 2008. Cytotoxic effects of dimethyl sulphoxide (DMSO) on cochlear organotypic cultures. *Hear Res,* 236**,** 52-60.

RAGHAVA, S., HAMMOND, M. & KOMPELLA, U. B. 2004. Periocular routes for retinal drug delivery. *Expert Opin Drug Deliv,* 1**,** 99-114.

READ, D. S., MCCALL, M. A. & GREGG, R. G. 2002. Absence of voltage-dependent calcium channels delays photoreceptor degeneration in rd mice. *Exp Eye Res,* 75**,** 415-20.

SAHABOGLU, A., PAQUET-DURAND, O., DIETTER, J., DENGLER, K., BERNHARD-KURZ, S., EKSTROM, P. A., HITZMANN, B., UEFFING, M. & PAQUET-DURAND, F. 2013. Retinitis pigmentosa: rapid neurodegeneration is governed by slow cell death mechanisms. *Cell Death Dis,* 4**,** e488.

SAKTI, D. H., CORNISH, E. E., NASH, B. M., JAMIESON, R. V. & GRIGG, J. R. 2023. IMPDH1-associated autosomal dominant retinitis pigmentosa: natural history of novel variant Lys314Gln and a comprehensive literature search. *Ophthalmic Genet,* 44**,** 437-455.

SANYAL, S. & BAL, A. K. 1973. Comparative light and electron microscopic study of retinal histogenesis in normal and rd mutant mice. *Z Anat Entwicklungsgesch,* 142**,** 219-38.

SCHMITZ, Y. & WITKOVSKY, P. 1997. Dependence of photoreceptor glutamate release on a dihydropyridine-sensitive calcium channel. *Neuroscience,* 78**,** 1209-16.

SCHOLL, H. P., STRAUSS, R. W., SINGH, M. S., DALKARA, D., ROSKA, B., PICAUD, S. & SAHEL, J. A. 2016. Emerging therapies for inherited retinal degeneration. *Sci Transl Med,* 8**,** 368rv6.

SZEL, A., ROHLICH, P., CAFFE, A. R., JULIUSSON, B., AGUIRRE, G. & VAN VEEN, T. 1992. Unique topographic separation of two spectral classes of cones in the mouse retina. *J Comp Neurol,* 325**,** 327-42.

TOLONE, A., BELHADJ, S., RENTSCH, A., SCHWEDE, F. & PAQUET-DURAND, F. 2019. The cGMP Pathway and Inherited Photoreceptor Degeneration: Targets, Compounds, and Biomarkers. *Genes (Basel),* 10.

TOLONE, A., HAQ, W., FACHINGER, A., ROY, A., KESH, S., RENTSCH, A., WUCHERPFENNIG, S., ZHU, Y., GROTEN, J., SCHWEDE, F., TOMAR, T., HERBERG, F. W., NACHE, V. & PAQUET-DURAND, F. 2023. The PKG Inhibitor CN238 Affords Functional Protection of Photoreceptors and Ganglion Cells against Retinal Degeneration. *Int J Mol Sci,* 24.

VIGHI, E., TRIFUNOVIC, D., VEIGA-CRESPO, P., RENTSCH, A., HOFFMANN, D., SAHABOGLU, A., STRASSER, T., KULKARNI, M., BERTOLOTTI, E., VAN DEN HEUVEL, A., PETERS, T., REIJERKERK, A., EULER, T., UEFFING, M., SCHWEDE, F., GENIESER, H. G., GAILLARD, P., MARIGO, V., EKSTROM, P. & PAQUET-DURAND, F. 2018. Combination of cGMP analogue and drug delivery system provides functional protection in hereditary retinal degeneration. *Proc Natl Acad Sci U S A,* 115**,** E2997-E3006.

VIRINGIPURAMPEER, I. A., GREGORY-EVANS, C. Y., METCALFE, A. L., BASHAR, E., MORITZ, O. L. & GREGORY-EVANS, K. 2019. Cell Death Pathways in Mutant Rhodopsin Rat Models Identifies Genotype-Specific Targets Controlling Retinal Degeneration. *Mol Neurobiol,* 56**,** 1637-1652.

YAN, J., GUNTER, A., DAS, S., MUHLFRIEDEL, R., MICHALAKIS, S., JIAO, K., SEELIGER, M. W. & PAQUET-DURAND, F. 2022. Inherited Retinal Degeneration: PARP-Dependent Activation of Calpain Requires CNG Channel Activity. *Biomolecules,* 12.

YANG, P., LOCKARD, R., TITUS, H., HIBLAR, J., WELLER, K., WAFAI, D., WELEBER, R. G., DUVOISIN, R. M., MORGANS, C. W. & PENNESI, M. E. 2020. Suppression of cGMP-Dependent Photoreceptor Cytotoxicity With Mycophenolate Is Neuroprotective in Murine Models of Retinitis Pigmentosa. *Invest Ophthalmol Vis Sci,* 61**,** 25.

ZWERNER, J. & FIORENTINO, D. 2007. Mycophenolate mofetil. *Dermatol Ther,* 20**,** 229-38.

8 Statement of Authorship

The work was performed at the Institute for Ophthalmic Research at the University Hospital of Tübingen under the supervision of Prof. Dr. rer. nat. François Paquet-Durand.

I assure that I wrote the manuscript myself and that I did not use any other sources than those I indicated.

Gießen, 10.03.2025

Peter Klaus Jenisch

Danksagung

Ich danke meinem Doktorvater, Herrn Prof. Dr. François Paquet-Durand, für die stets hervorragende und freundliche Betreuung, die wegweisenden Anregungen, sowie das Überlassen des Themas und die interessanten Gespräche.

Für die ständige Hilfsbereitschaft im Labor bei der Vorbereitung meiner Versuche und die praktischen Tipps bei der Durchführung bedanke ich mich bei allen Mitgliedern des Labors, für ihre Hilfe und die gute Zeit, die wir gemeinsam beschritten haben. Insbesondere möchte ich Norman Rieger für stetige Hilfe bei Experimenten, Yu Zhu für die Bereitstellung ihrer Zeichnungen und Lan Wang für das Überlassen kultivierter Retinaschnitte danken.

Weiterhin danke ich Viet Chau, Heiko, Christian und Felix für das Korrekturlesen dieser Arbeit und hilfreichen Ideen, als auch für die Begleitung meiner Freunde durch Studium und Arbeit.

Ein besonderer Dank gilt meiner Partnerin Schérine Olbrich, welche mich über die gesamte Zeit der Arbeit motiviert und unterstützt hat.

Abschließend bedanke ich mich bei meiner Familie, ohne deren Unterstützung ich nicht so weit gekommen wäre.